Charge Conductivity in Donor-Acceptor Polymer Dispersions Measured with Time-Resolved Terahertz Spectroscopy

*Timothy J. Magnanelli and Edwin J. Heilweil**

Physical Measurement Laboratory, National Institute of Standards and Technology (NIST), Gaithersburg, MD, 20899, USA

Corresponding Author

***** Edwin J. Heilweil; (301) 975-2370; edwin.heilweil@nist.gov

ABSTRACT Ultrafast Time-Domain and Time-Resolved Terahertz (TDS/TRTS) spectroscopic methods are utilized to explore photoconductive properties of five conjugated donor-acceptor co-polymers (PCDTPT, CDTBTZ, IDTBT, PBDTTPD and N2200) dispersed in room temperature toluene, a nonpolar dielectric solvent. TRTS provides an effective non-contact handle to interrogate localized relative conductivity of dispersed co-polymers. Conductivity dynamics are contrasted among disparate polymer structures and between their photoconductive peak and thermalized time-delayed signatures. Photoconductivity kinetics, relative levels of real/imaginary conductivity, and carrier properties are summarized with higher energy photoexcitation increasing the real photoconductivity by up to three-fold. Molecular orbital pictures and donor-acceptor twisting mode frequencies ascertained through *ab initio* calculations (*via* Density Functional Theory) support descriptions of the relative efficacies of charge transfer from the perspective of the localized THz method.

TOC GRAPHIC

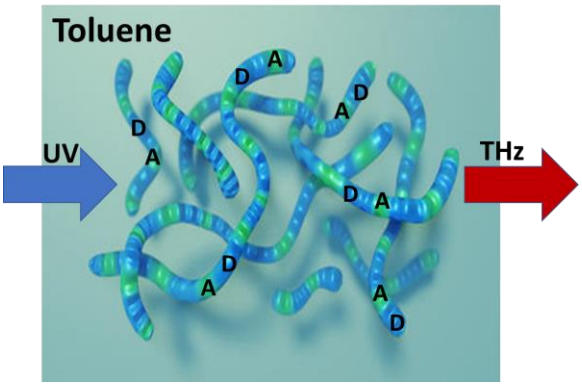

KEYWORDS: donor-acceptor polymers; liquid dispersions; localized conductivity; time-resolved terahertz; ultrafast THz spectroscopy

Introduction

Donor-acceptor (D-A) co-polymers represent a powerful extension from traditional conjugated polymers for promoting efficient charge transfer in photovoltaic and electronic devices. Specific synthetic design of intrinsic chromophores,[1–4] solubilizing substituents,[5,6] and relative orientations and structures of co-polymer films[7–9] has been found to facilitate charge and energy transfer. Improved charge transfer largely occurs through modification of respective donor/acceptor energy levels and delocalization,[3,4,10] intramolecular dynamics,[2] and intermolecular stacking, packing, and morphological patterns.[5,6] Organic field effect transistors (OFETs) and organic photovoltaic devices (OPVs) utilizing an active layer of a conjugated polymer are often the endpoint for testing the viability and efficiency of the material.[6,11,12] These devices provide effective and straightforward comparisons and ultimately represent the end-use of the polymer (or mixtures) while incorporating the effects of morphology (intermolecular order and stacking), grain boundaries, crystalline domain formation, and defects into the resulting charge propagation or harvesting efficiencies.[13]

Alternatively, all-optical spectroscopic methods such as time-resolved microwave conductivity (TRMC)[14–16] and time-resolved terahertz spectroscopy (TRTS)[17–19] provide non-contact measures of photoinduced conductivity. They have been used to characterize conductivity in thin-film layers of conjugated polymers without applying contacts or fabricating devices, permitting greater repeatability and improving ease of assessment.[20,21] They are also differentially sensitive to larger and smaller domains of the material, respectively, and we focus on the latter (TRTS) herein.[22,23] As compared with contact measurements and TRMC, TRTS is a more localized measure of conductivity that reports higher charge mobility by avoiding the effects of grain boundaries, site defects/traps, and other limitations on primarily long-distance

charge motion. TRTS reports on the aggregate charge mobility of photogenerated electrons and holes through their interaction with the complex dielectric function of THz light *via* its complex refractive index. This is reflected by equations presented in previous work considering films in which the difference in dielectric permittivity (with and without photoexcitation present) can be related quantitatively to photoconductivity and charge mobility of generated polarons in polymeric samples.[20]

While thin films incorporate numerous flexible properties influenced by modifying the constituent polymers or fabrication conditions, including solvent selection and annealing,[19,24,25] they represent an additional degree of uncertainty that can hinder repeatability. As presented here, a rapid and simplified approach for examining intramolecular conduction dynamics would prove beneficial for interrogating the photoconductivity of target polymers in a nonpolar dielectric medium (i.e. dispersed in a nonpolar solvent). TRMC was previously shown to illustrate differences in photoconductivity between MEH-PPV, P3HT, and other polymers over delocalized domains.[14,15] To our knowledge, only one previous study of a dispersed conducting polymeric system (MEH-PPV in benzene) using TRTS was conducted where very weak quantum efficiency (*ca.* 10^{-5}) and conductivity were reported.[26] It was also estimated in that work that the nearest neighbor distance between polymers was approximately 20 nm for a 2.6 mg/mL solution, implying an ample solvation shell to ensure completely physical (and electronic) isolation.[26]

Our initial study used TRTS to examine photoinduced conductivity of the D-A co-polymer (PCDTPT) as an oriented anisotropic film and dispersed in toluene.[20] In this work we explore representative dispersed co-polymers with different structures that yield measurable TRTS conductivity signals to confirm its general applicability. This approach is not viable for every

photoconductive polymer, particularly those that rely on intermolecular charge interactions or contact with electron acceptors to stabilize charge separation (i.e. for P3HT and PBTTT mixed with PCBM in films).[22,27] Of note, we were unable to obtain TRTS signals from P3HT and PBTTT in toluene or dispersed in chlorinated solvents, as reported previously.[20] PCDTPT also photodegraded and yielded no signal when dispersed in chlorinated solvents due to charge quenching/stabilization and free radical catalyzed reactions.[16] Each polymer examined in this work readily dispersed into THz-transparent toluene solvent. We estimate the nearest neighbor distances for the samples studied to range from 40 nm to 85 nm suggesting the dispersed polymers are well isolated (assuming complete solvation with *ca.* 10^6 solvent molecules per polymer strand *ca.* 100 D-A units long).

Investigated Polymers

Figure 1 illustrates the structures of five sample D-A co-polymers considered here and their UV-Vis-NIR electronic absorption spectra when dispersed in toluene. These co-polymers have been utilized for their photoconductive behavior in past works and are referred to by shorthand names CDTBTZ (C),[5,12] PCDTPT (PC),[12,20] IDTBT (I),[11,28–30] PBDTTPD (PB),[6,31] and N2200 (N)[32] with full IUPAC names listed in the supplementary information (SI). Each polymer exhibits a low-lying absorption band corresponding to a donor-acceptor charge transfer state with center wavelength ranging from ≈ 600 nm for (PB) to ≈ 875 nm for (PC). These bands are directly interrogated for (C), (PC), and (N) using 800 nm photoexcitation pulses. All co-polymers (except (PC)) are compared *via* 400 nm photoexcitation resonant with the higher-lying conjugated thiophene (or cyclopentadiene)-based π-π* transition of each donor moiety.

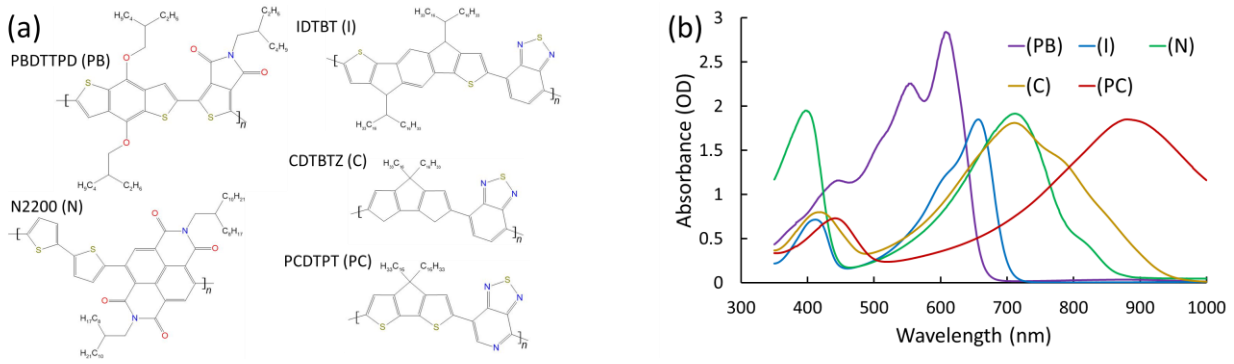

Figure 1. (a) Structures of D-A- co-polymers (PB), (I), (N), (C), and (PC). The orientation of the nitrogen along the (PC) backbone is random. (b) UV-Vis-NIR electronic absorption spectra dispersions of each donor-acceptor co-polymer in room temperature toluene at densities of 0.5 mg/mL (0.2 mg/mL for (PC)) and 1 mm pathlength.

TRTS Methodology

Each co-polymer's photoconductivity and time-dependent dynamics are obtained through TRTS measurements.[20] Using 400 nm or 800 nm excitation pulses (*ca.* 40 fs FWHM) with gated time-delayed THz probe pulses (spanning ≈ 0.3 THz to 2.25 THz; 0.5 ps FWHM), conductivity TRTS traces are collected and peak normalized for analysis.

Results and Discussion

Representative, integrated TRTS photoconductivity data collected as a function of pump-probe time delay is displayed as Figure 2 for each of the five co-polymers considered here. Figure 2(a) shows the normalized time-dependent results (for photon flux and polymer concentration) on an absolute level of photoconductivity, while Figure 2(b) sets the traces in Figure 2(a) on a globally

relative scale (peak signal set to 1) for direct kinetic comparison. The solid traces indicate fits to the kinetic data by a convoluted bi-exponential decay model. Though these fits are primarily empirical, we loosely assign the first decay lifetime to ultrafast (<1 ps) geminate recombination of separated charges and the second, longer lifetime to a mixture of vibrational relaxation, charge trapping, and additional charge recombination (10's of ps). Parameters and fitting values associated with a bi-exponential model (convoluted with an instrument response function) applied to the data sets are included in Table S1 of the SI. Quantitative comparison of these parameters is plausible but we avoid placing too much emphasis on this given the inherently nonexponential nature of photodynamics in polymers. The inherent large-scale motions of dispersed polymers give rise to heterogeneous ensembles of responses based on many accessible variations in local polymer configuration (further discussion is reserved for the SI).

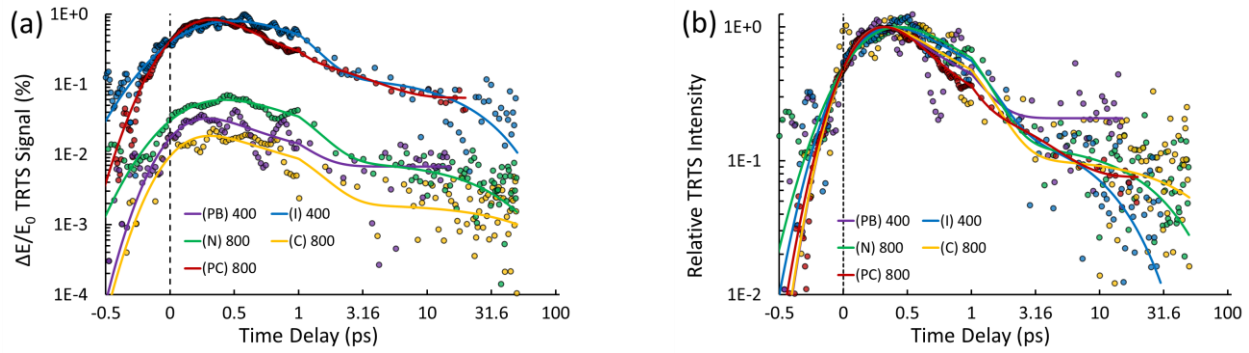

Figure 2. Time dependence of the frequency-integrated TRTS conductivity for (PB), (I), (N), (C), and (PC) normalized to (a) a constant input photon flux (1 W/cm^2 and 0.5 W/cm^2 for 400 nm and 800 nm, respectively) and D-A monomer concentration (1*10^{17} monomers/cm^2*mm pathlength) and (b) the highest modeled signal. The pump wavelength (nm) for each system is conveyed in the key. The time-delay axis is linear until 1 ps and logarithmic beyond (1 ps to 100 ps) while the TRTS signal is also presented on a logarithmic scale (omitting negative intensity points). Data points beyond 1 ps were averaged in groups of 20 for clarity. Fits to a convoluted bi-exponential kinetic model are indicated by the traces with associated parameters reported in the SI.

From Figure 2(a), (I) and (PC) are clearly more conductive than the remaining three, though this result may be influenced by the pump energy used (400 nm vs. 800 nm). We reserve further consideration of this pump dependence and other absolute metrics of photoconductivity in the subsequent frequency-dependent analyses. After photoexcitation, all polymers exhibit a rapid initial "peak" conduction decay (< 1 ps) before plateauing or slowly decreasing at longer time delays (Figure 2(b)). (N) and (I) show slightly longer initial decays than the others. (PB) exhibits a pronounced constant time-delayed "tail" signature that cannot be modeled by a second decay lifetime over the observed timescale. This suggests that 400 nm excitation of (PB) minimizes charge recombination proportionally to how many THz responsive transients were initially generated.[31] Kinetic comparisons using the same excitation energy for all of the polymers would be necessary to make this claim more definitive, but the trend does stand out within the representative data shown. We also suggest that excitation of conducting polymers near their absorptive band edge would be a follow-on study to obtain more critical and comparative information concerning these and related systems.

We now evaluate absolute conductivity from signal intensities (real and imaginary) determined from THz time-dependent waveforms (TDS) obtained at "peak" and "tail" delays (*ca.* 0.4 and 20 ps, respectively) shown in Figure 2. The frequency-dependent conductivity is extracted by complex Fourier Transform (FFT) of the photoinduced response. Figure 3 displays normalized frequency-dependent conductivity for 400 nm excitation of (PB), (I), (N), and (C) and previously reported 800 nm excitation of (PC).[20] Unfortunately, 400 nm photoexcitation could not be applied to (PC) as no co-polymer sample remained following the aforementioned study.[20] For systems where carrier motion exhibits significant high frequency rebounding, the standard Drude conductivity model must be extended to account for positive real and negative

imaginary conductivity. The Drude-Smith model incorporates an extra term (the c_1 parameter) to the Drude model to signify the likelihood of rebounding (e.g., 0 for pure Drude conductivity, -1 for fully confined charge motion) and is typically applied to conducting polymers.[17] Fitting these co-polymer conductivity traces to the Drude-Smith model (Equation (1))[17,20] permits relating spectral shapes to differences in conductive properties, including scattering times (τ) and backscattering (c_1) parameters.

$$\sigma(\omega) = C_\sigma * \frac{\tau}{(1 - i\omega\tau)} * \left(1 + \frac{c_1}{(1 - i\omega\tau)}\right) \quad (1)$$

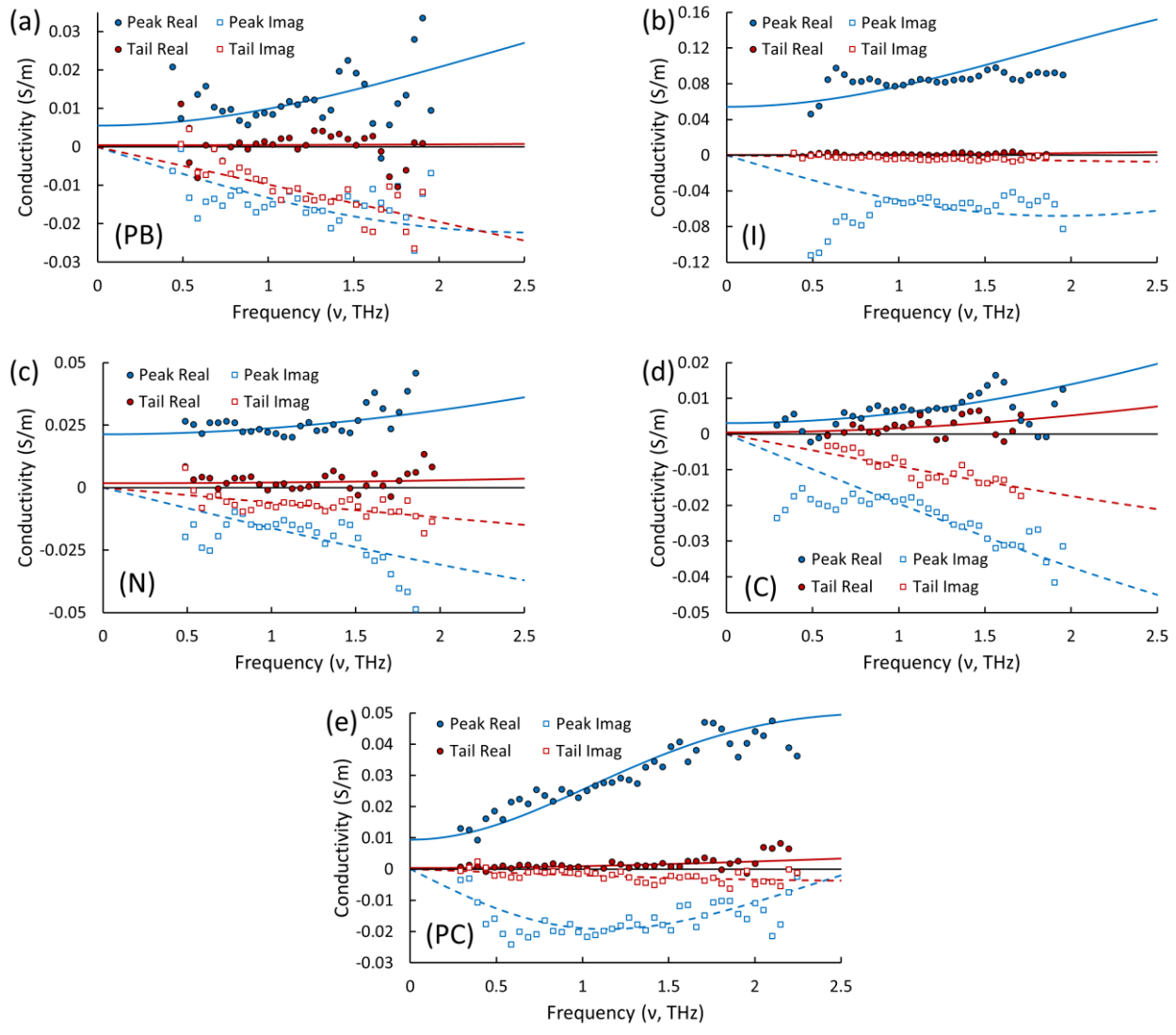

Figure 3. Frequency-dependent THz conductivity with 400 nm excitation of (a) (PB), (b) (I), (c) (N), and (d) (C) and previously reported 800 nm excitation of (e) (PC).[20] Real (solid circles/line Drude-Smith fits) and imaginary conductivity (open squares/dashed line Drude-Smith fits) for the peak (blue) and tail (red) delays are normalized to $5*10^{16}$ absorbed photons/cm^3 across a 1 mm pathlength. (N) and (C) 800 nm excitation results are included in the SI (Figure S1).

We observe significant peak conductivity values for each D-A co-polymer. Tail signatures for (PB), (N), and (C) yield τ approaching zero (i.e. flat/near-zero real and linear negative imaginary response over the frequency range), indicating net conduction occurs over extremely localized distances.[26] This limiting case implies highly localized electron-hole charge distributions (excitons or polarons) which effectively rebound (e.g., very small τ and near $c_1 = -1$ Drude-Smith values) at significantly higher frequency than probed within the THz range (e.g., >>2 THz).[17] This situation occurs for confined excitons following co-polymer relaxation,[21] a fast-scattering limit for plasmons,[33] and in P3HT films assessed using TRTS[22] suggesting that excitons/polarons are confined to nm length scales. As observed previously,[20] some data as in Figure 3(b), exhibit noteworthy deviations from the Drude-Smith model fit, largely reflected as more negative imaginary conductivity below 1 THz. This is primarily attributable to spatial spectral chirp of the THz probe (lowest frequencies on the outside edge of the beam) and a resulting slight mismatch in overlap with the 400 nm or 800 nm photoexcitation pulse. The resulting effect on the Drude-Smith model fit itself is minimal given the limited leverage of these points because the model fit must go to zero imaginary intensity at 0 THz.

Drude-Smith fit parameters and values for the peak traces shown in Figure 3 are included in Table 1 below. Additional Drude-Smith fit parameters associated with the corresponding tail traces and additional, unshown datasets are included in a complete table in the SI (Table S2). These parameter fits can provide a limited quantitative comparison of conductive properties of

the co-polymers for instances with significant spectral curvature and where the model is not an over-representation of the observed behavior (as occurs with many tail spectra). The absolute photoconductivity scales roughly as the product of the pre-factor (C_σ) and scattering time (τ), while the backscattering parameter (c_1) indicates the degree of intrachain scattering of charges within the co-polymer. From this perspective, we find that (PB) is the least conductive and (C) the most "confined" at the photoconductivity peak, while charges in (I) are the most conductive and labile. As the long-time tail traces are more important to consider for practical applications of co-polymers in photoactive and electronic devices and fit parameters are not as robust for these datasets as for the peak responses, we instead consider a more direct comparison of the relative complex photoconductivity.

Table 1. Drude-Smith model best fit parameter values for frequency-dependent data at peak photoexcitation shown in Figure 3 and based on Equation 1. Parenthetical quantities represent the 95% confidence interval range for each with "U" indicating the parameter being unbounded with 95% confidence in that direction (Type A, k = 1.96 error analysis).

Polymer / Pump λ (nm)	**(PB) / 400**	**(I) / 400**	**(N) / 400**	**(C) / 400**	**(PC) / 800**
C_σ	1.21 (0.30 – U)	3.60 (0.957 – U)	6.96 (1.13 – U)	7.62 (1.65 – U)	1.63 (1.31 – 2.13)
τ	24.9 (0.6 – 53.0)	31.4 (0.1 – 79.3)	11.7 (0.4 – 31.5)	11.3 (1.3 – 25.0)	54.7 (46.0 – 63.4)
c_1	-0.946 (-1 – -0.91)	-0.865 (-0.98 – -0.82)	-0.920 (-0.98 – -0.90)	-0.989 (-1 – -0.98)	-0.905 (-0.94 – -0.87)

By averaging the real or imaginary conductivity magnitude from the Drude-Smith model fits (Equation 1) extrapolated beyond the probe frequency range (0 to 2.5 THz), we quantitatively compare the relative photoconductivity between different polymers. Figure 4(a) presents log-scale average (THz) conductivity values obtained directly from the data shown in Figures 3 and S1 where normalization is based on the density of absorbed photons. Figure 4(b)

shows an analogous comparison where photoconductivity is normalized to a fixed incident photoexcitation fluence applied to a dispersion of fixed concentration of donor-acceptor monomeric units. As a note, the high absorbances of (N) at 400 nm and (PC) at 800 nm (Figure 1(b)) suggest that the normalization metric in Figure 4(b) could be slightly less accurate or produce a non-linearity if too much sample is present producing saturated light absorption. However, the first metric is consistent regardless of the specific sample OD as only the total absorbed photon density (rather than uniformity of excitation) matters for scaling. We present each metric as contrasting ways to view normalization of the polymer conductivity, either as a constant amount of light absorbed in Figure 4(a) for spectroscopic purposes or a fixed amount of light (energy) presented to a constant sample mass in Figure 4(b) for purposes of material utilization in application areas.

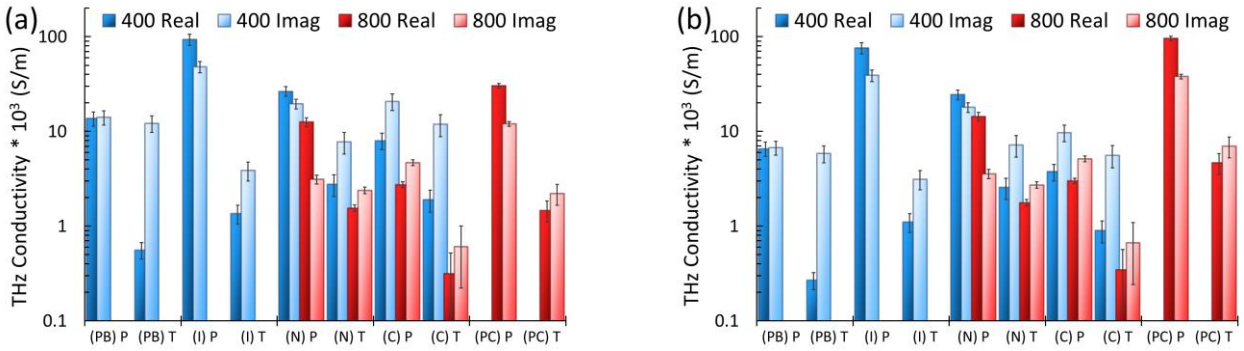

Figure 4. Conductivity of D-A co-polymers at their peak (P) photoconductive signal and vibrationally relaxed tail (T). These were normalized to (a) an absorbed excitation fluence of $5*10^{16}$ photons/cm^3 and (b) an incident photon density of 10 mJ/cm^2 and donor-acceptor monomer unit concentration of 1 µmol/cm^3. Conductivities are multiplied by 1000 and error bars signify 95% confidence intervals associated with each value (Type A, k = 1.96 error analysis).

When comparing conductivity values, we assume the real conductivity represents charges exhibiting a net dipole which absorb throughout the probe range (indicating charge motion). By contrast, the imaginary conductivity reflects modification to the phase of the THz probe field by

charges present whether in motion or not (i.e., delocalized across a 'polaron' with no net dipole). From this perspective, we examine the relative conductivity magnitudes between the co-polymers as a means of comparing the behavior of charges along their backbones. The largest to smallest real conductivity is (I) > (N) > (PB) > (C) for 400 nm excitation probed at the photoconductive peak and (N) ≥ (C) ≥ (I) > (PB) during the thermalized tail. The prominent peak conductivity for (I) indicates either a high initial charge yield or a pronounced initial charge mobility (leading to greater charge separation); at later delays, the well-conjugated backbone either permits substantial charge recombination and relaxation (by 20 ps) or rapid motion to trap sites, leaving few remaining free carriers. Conversely, with ≈1/3 the original generation efficiency as (I), (N) exhibits a significant leveling in both real and imaginary conductivity indicating better maintenance of charge motion and stabilization of charges beyond the initial excitation. (C) and particularly (PB) show minimal loss of imaginary conductivity despite a sizable decrease in the real conductivity, indicating stabilization of trapped, immobile charges following initial relaxation. This is potential evidence for stabilization of thermalized charges by recombination and the presence of excitons that exhibit some degree of polarizability or ability to interact with the electric field of the THz probe. The inability of these two polymers to stabilize/solvate one of the charges (electrons or holes) is the likely cause of this phenomenon as evidenced by their minimal efficiency when used without an accompanying donor/acceptor system.[12,31]

For 800 nm photoexcitation, the order from highest to lowest conductivity is (PC) > (N) > (C). This comparison corroborates a previous report that (PC) exhibits ≈10x better conductivity and performance in blade-coated OFETs than similarly-structured (C),[12] which agrees well with the observed ≈20x and ≈5x higher real conductivity values, respectively. Comparison between

400 nm and 800 nm photoexcitation of (N) and (C) reveals approximately half the photoconductivity efficiency in the latter (even less in (C) tail). This suggests improved and more labile charge generation via absorption of extra energy per photon and thereby facilitates greater initial charge motion/separation (real peak conductivity). This also inhibits subsequent charge recombination while promoting separate trapping, limited mobilization, and localization of the charges (maintaining tail conductivity). Additional relaxation of the photoconductive signal is observed at the latest time delays in Figure 2. Comparison as a function of pump energy would be necessary to confirm this suggestion, but the presence of higher tail conduction between each 400 nm and 800 nm dataset, where applicable, in Figure 4 suggests that this effect persists out to 10's of picoseconds, where additional pump energy-dependent localization still occurs.

Concerning each normalization metric, Figure 4(a) is useful when comparing charge yield following excitation while Figure 4(b) produces conductivity values comparable to casting an amount of co-polymer into a film (omitting intermolecular effects) under fixed irradiance. The two representations reveal slight relative differences between the polymers: 400 nm efficiency by the latter metric decreases for (PB), (C), and (I) and dramatically increases for (PC) relative to a *ca.* constant conductivity in (N) (on the scale selected).. In fact, (PC) experimentally produced the largest absolute photoconductivity signals for all polymer measurements.

Density Functional Theory Modelling

We also compared the above TRTS conductivity results to *ab initio* molecular orbital and vibrational frequency calculations. Here, we use Density Functional Theory (DFT) at the B3LYP/6-31G level of computation using GAMESS.[34] DFT has been utilized on oligomeric

segmented conjugated polymers to estimate bandgaps and highest occupied/lowest unoccupied molecular orbitals (HOMO/LUMO) energies,[3,10,35–38] predict stacking patterns,[5,39] and provide comprehensive overviews of electronic/vibrational characteristics including excited state delocalization.[40]

HOMO/LUMO Molecular Orbitals: The lowest energy optimized structures and HOMO/LUMO electron densities for each co-polymer D-A-D-A dimer unit (except (C)) are shown in Figure 5 with orbital energies given in SI Figure S2. The near-planar (PC) and (I) structures support delocalized HOMO electron density across the conjugated D-A-D backbone segment while the (PB) and (N) structures place HOMO density predominantly on the donor. (PC) and (N) exhibit LUMOs that occupy both acceptor units, (PB) does as well though asymmetrically across several orbitals, and (I)'s LUMO yields localization predominantly on a single acceptor. These findings support the TRTS result that (N) exhibits a pronounced (relatively high) real conductivity for the long-time tail compared to the photoconductive peak; here, the HOMO/LUMO orbital density occurs across numerous monomeric segments while maintaining disparate localization on donor/acceptor moieties compared to all other (more delocalized) systems. Localized LUMO density on the acceptor may also support the largest peak conductivities for (I) and (PC). At the D-A molecular level, one may surmise that these measures of localized, intramolecular photoconductivity (peak and tail TRTS) can be compared in conjunction with computational modeling. This metholodology provides access to unique information by utilizing a novel experimental domain (nearly isolated polymer strands) between the direct analysis of optoelectronic properties of thin films or devices and pure computation. Additional comparisons of orbital diagrams obtained for single D-A segments are included as Figure S3 of the SI.

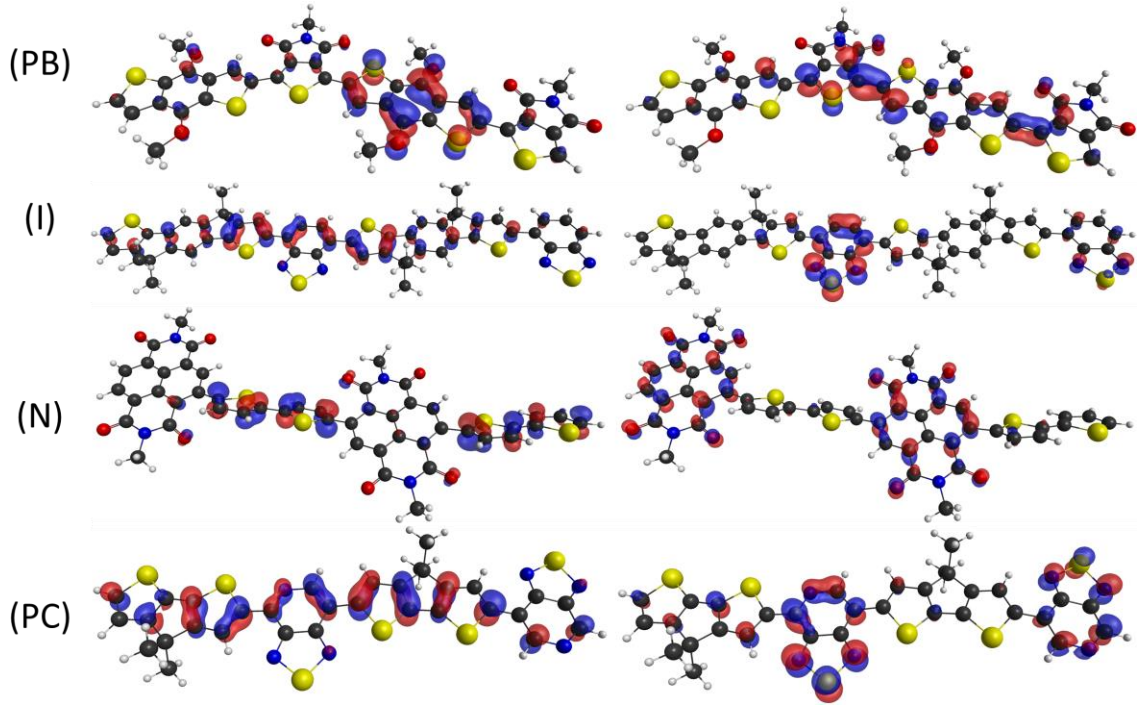

Figure 5. Calculated HOMO (left) and LUMO (right) molecular orbitals for (PB), (I), (N), and (PC) D-A-D-A oligomeric units ((PC) and (C) are nearly identical). Equivalent comparison of optimized D-A monomeric segments is included in the SI (Figure S3).

D-A Torsional Mode Frequencies: The limiting case of nanometer exciton and polaron confinement potentially implies that the "charge transfer" electronic state couples to internal vibrational degrees of freedom (large amplitude backbone torsional or high frequency D-A twisting modes) that directly affect the local atomic structure, conjugation and conductivity.[16, 17] They may also depend on inherent properties of the donor/acceptor structure including D-A offset angle and relative molecular masses (which affect vibrational mode frequencies). For instance, an "along chain" D-A torsional mode with non-zero intensity is estimated from the DFT calculations for (PC) to occur at 166 cm^{-1} (5 THz). This similar mode occurs at higher frequencies for (I) and (C) and lower frequencies for (PB) and especially (N) (with three similar

D-A torsional modes) as summarized in Table 2. With the exception of (N), which exhibits the largest (relative) real tail conductivity and lowest torsional frequency, the DFT-estimated D-A backbone torsional frequencies purport the crude trend that smaller effective real and dominant imaginary components occur for localized conductivity as the twisting frequency increases.

It is interesting to note that (N) has several structural and electronic features that differ from the other polymers which may cause it to deviate from the aforementioned trend and affect the measured THz conductivity. These include having a significantly larger conjugated acceptor moiety, an inherently pronounced (>30°) non-planar D-A backbone angle which may isolate electron/hole density onto acceptor/donor segments more readily, and the lowest estimated HOMO energy (see Figure S2). (N) is also considered an n-type semiconductor (preferentially stabilizing and transporting electrons) rather than all others which are considered p-type (primarily hole transporters). This may permit higher charge conductivity within the "localized" donor through more mobile conjugated electron transport that yields higher signals. However, confirmation of this possibility requires further investigation of additional polymeric materials, particularly those that are n-type.

At the other extreme, intense D-A twisting modes for PBTTT and P3HT occur at 648 cm^{-1} and 840 cm^{-1} (>19 THz)[41] significantly above our observation window. Indeed, we did not measure any TRTS signals for structurally simpler and less massive P3HT and PBTTT perhaps because their backbone torsional frequencies are much higher than for the D-A co-polymers considered here.

Table 2. DFT calculated backbone torsional twisting frequencies and measured peak and tail real conductivity (Figure 4a) using 400 nm photoexcitation of each co-polymer contrasted with PBTTT and P3HT. (PC) results were collected using 800 nm photoexcitation.

Polymer (DA Dyad)	(N)	(PB)	(I)	(PC)	(C)	PBTTT	P3HT[41]
Twist frequency (cm^{-1})	~65	108	156	166	206	648	830
Twist frequency (THz)	2	3.2	4.7	5	6.2	19.4	24.9
Tail Real σ ($S/m*10^{-3}$)	2.77	0.56	1.36	1.47	1.91	0	0
Peak Real σ ($S/m*10^{-3}$)	26.6	13.7	93.6	30.4	8.0	0	0

Conclusions

Five D-A co-polymers dispersed in toluene yielded quantifiable, photoconductive TRTS signals. Assessments of photoconductivity for each molecular structure suggest highly localized exciton/polaron formation following picosecond recombination and thermal equilibration. The Drude-Smith carrier rebound model adequately fits the frequency response at the photoconductive peak and 20 ps time-delay after photoexcitation, permitting inter-comparison of the THz frequency range conductivity. In cases with near-infrared and near-UV absorption, 400 nm photoexcitation significantly increases photoconductivity over equivalent (per photon) 800 nm photoexcitation. Normalized frequency-dependent comparisons between co-polymers permits qualitative descriptions of their conductive properties and relative efficiencies. (PC) and (N) show higher photoconductivity than (C) and (PB), particularly at long time delays, and (I) photoconductivity varies most substantially with time delay. Interrogating effects of tunable excitation on conductivity within the charge transfer band, particularly near the band edge, and of dispersing the co-polymers in other solvents would be worthwhile follow-up studies for these and other materials.

Several systems exhibit near-zero real photoconductivity with strong imaginary components implying highly localized (rebounding) charged pair motion within short (nm) distances along the chain. These responses generally correspond to trends in the molecular orbital profiles and

coupling to high frequency backbone torsional modes, especially those which produce no photoconductive response. Examination of *ab initio* theoretical models corroborates tendencies in photoconductivity, but further calculations are suggested to explore detailed structure-function relationships between dispersed polymers and TRTS conductivity measurements. This combined methodology occupies a unique space for experimentally interrogating the intramolecular photoconductive dynamics of D-A co-polymers while avoiding device fabrication/film-casting and intermolecular (morphological) polymer interaction effects and maintaining amenability to computational comparisons.

ASSOCIATED CONTENT

A Supplemental Information file (PDF) contains acronyms, TRTS exponential model and TRTS-TDS Drude-Smith model fit parameters, predictions of bandgaps/delocalization and HOMO/LUMO energies, DFT D-A monomeric unit molecular orbital visualizations, and calculated infrared frequencies, intensities and structural D-A "torsional" mode vectors.

AUTHOR INFORMATION

The authors declare no competing financial interests.

ACKNOWLEDGMENTS

This work was supported by internal NIST (National Institute of Standards and Technology) STRS (Scientific Technical and Research Services). T. J. M. gratefully acknowledges support from the NIST/National Research Council (NRC) postdoctoral associates' program. We kindly thank L. J. Richter and J. Smith for providing (C), (PC), (N) and (I) samples for study.

References

(1) Haid, S.; Marszalek, M.; Mishra, A.; Wielopolski, M.; Teuscher, J.; Moser, J.-E.; Humphry-Baker, R.; Zakeeruddin, S. M.; Grätzel, M.; Bäuerle, P. Significant Improvement of Dye-Sensitized Solar Cell Performance by Small Structural Modification in π-Conjugated Donor–Acceptor Dyes. *Advanced Functional Materials* **2012**, *22* (6), 1291–1302. https://doi.org/10.1002/adfm.201102519.

(2) Etzold, F.; Howard, I. A.; Forler, N.; Melnyk, A.; Andrienko, D.; Hansen, M. R.; Laquai‡, F. Sub-Ns Triplet State Formation by Non-Geminate Recombination in PSBTBT:PC70BM and PCPDTBT:PC60BM Organic Solar Cells. *Energy Environ. Sci.* **2015**, *8* (5), 1511–1522. https://doi.org/10.1039/C4EE03630A.

(3) Zhuang, W.; Lundin, A.; Andersson, M. R. Computational Modelling of Donor–Acceptor Conjugated Polymers through Engineered Backbone Manipulations Based on a Thiophene–Quinoxaline Alternating Copolymer. *J. Mater. Chem. A* **2014**, *2* (7), 2202–2212. https://doi.org/10.1039/C3TA14456A.

(4) Popere, B. C.; Della Pelle, A. M.; Thayumanavan, S. BODIPY-Based Donor–Acceptor π-Conjugated Alternating Copolymers. *Macromolecules* **2011**, *44* (12), 4767–4776. https://doi.org/10.1021/ma200839q.

(5) Pisula, W.; Tsao, H. N.; Dudenko, D.; Cho, D. M.; Puniredd, S. R.; Zhao, Y.; Mavrinskiy, A.; Shu, J.; Hansen, M. R.; Baumgarten, M.; Müllen, K. Solid-State Organization and Ambipolar Field-Effect Transistors of Benzothiadiazole-Cyclopentadithiophene Copolymer with Long Branched Alkyl Side Chains. *Polymers* **2013**, *5* (2), 833–846. https://doi.org/10.3390/polym5020833.

(6) Constantinou, I.; Lai, T.-H.; Klump, E. D.; Goswami, S.; Schanze, K. S.; So, F. Effect of Polymer Side Chains on Charge Generation and Disorder in PBDTTPD Solar Cells. *ACS Appl. Mater. Interfaces* **2015**, *7* (48), 26999–27005. https://doi.org/10.1021/acsami.5b09497.

(7) Hung, Y.-C.; Chao, C.-Y.; Dai, C.-A.; Su, W.-F.; Lin, S.-T. Band Gap Engineering via Controlling Donor–Acceptor Compositions in Conjugated Copolymers. *J. Phys. Chem. B* **2013**, *117* (2), 690–696. https://doi.org/10.1021/jp3090974.

(8) Chen, K.-S.; Zhang, Y.; Yip, H.-L.; Sun, Y.; Davies, J. A.; Ting, C.; Chen, C.-P.; Jen, A. K.-Y. Highly Efficient Indacenodithiophene-Based Polymeric Solar Cells in Conventional and Inverted Device Configurations. *Organic Electronics* **2011**, *12* (5), 794–801. https://doi.org/10.1016/j.orgel.2011.02.004.

(9) Zhu, Z.; Waller, D.; Gaudiana, R.; Morana, M.; Mühlbacher, D.; Scharber, M.; Brabec, C. Panchromatic Conjugated Polymers Containing Alternating Donor/Acceptor Units for Photovoltaic Applications. *Macromolecules* **2007**, *40* (6), 1981–1986. https://doi.org/10.1021/ma062376o.

(10) Blouin, N.; Michaud, A.; Gendron, D.; Wakim, S.; Blair, E.; Neagu-Plesu, R.; Belletête, M.; Durocher, G.; Tao, Y.; Leclerc, M. Toward a Rational Design of Poly(2,7-Carbazole) Derivatives for Solar Cells. *J. Am. Chem. Soc.* **2008**, *130* (2), 732–742. https://doi.org/10.1021/ja0771989.

(11) Nikolka, M.; Nasrallah, I.; Rose, B.; Ravva, M. K.; Broch, K.; Sadhanala, A.; Harkin, D.; Charmet, J.; Hurhangee, M.; Brown, A.; Illig, S.; Too, P.; Jongman, J.; McCulloch, I.; Bredas, J.-L.; Sirringhaus, H. High Operational and Environmental Stability of High-

Mobility Conjugated Polymer Field-Effect Transistors through the Use of Molecular Additives. *Nature Materials* **2017**, *16* (3), 356–362. https://doi.org/10.1038/nmat4785.
(12) Wu, D.; Kaplan, M.; Ro, H. W.; Engmann, S.; Fischer, D. A.; DeLongchamp, D. M.; Richter, L. J.; Gann, E.; Thomsen, L.; McNeill, C. R.; Zhang, X. Blade Coating Aligned, High-Performance, Semiconducting-Polymer Transistors. *Chem. Mater.* **2018**, *30* (6), 1924–1936. https://doi.org/10.1021/acs.chemmater.7b04835.
(13) McCullough, R. D.; Williams, S. P. Toward Tuning Electrical and Optical Properties in Conjugated Polymers Using Side-Chains: Highly Conductive Head-to-Tail, Heteroatom Functionalized Polythiophenes. *J. Am. Chem. Soc.* **1993**, *115* (24), 11608–11609. https://doi.org/10.1021/ja00077a074.
(14) Grozema, F. C.; Siebbeles, L. D. A.; Warman, J. M.; Seki, S.; Tagawa, S.; Scherf, U. Hole Conduction along Molecular Wires: σ-Bonded Silicon Versus π-Bond-Conjugated Carbon. *Advanced Materials* **2002**, *14* (3), 228–231. https://doi.org/10.1002/1521-4095(20020205)14:3<228::AID-ADMA228>3.0.CO;2-3.
(15) Grozema, F. C.; van Duijnen, P. Th.; Berlin, Y. A.; Ratner, M. A.; Siebbeles, L. D. A. Intramolecular Charge Transport along Isolated Chains of Conjugated Polymers: Effect of Torsional Disorder and Polymerization Defects. *J. Phys. Chem. B* **2002**, *106* (32), 7791–7795. https://doi.org/10.1021/jp021114v.
(16) Hoofman, R. J. O. M.; de Haas, M. P.; Siebbeles, L. D. A.; Warman, J. M. Highly Mobile Electrons and Holes on Isolated Chains of the Semiconducting Polymer Poly(Phenylenevinylene). *Nature* **1998**, *392*, 54–56.
(17) Ulbricht, R.; Hendry, E.; Shan, J.; Heinz, T. F.; Bonn, M. Carrier Dynamics in Semiconductors Studied with Time-Resolved Terahertz Spectroscopy. *Reviews of Modern Physics* **2011**, *83* (2), 543–586. https://doi.org/10.1103/RevModPhys.83.543.
(18) Knoesel, E.; Bonn, M.; Shan, J.; Wang, F.; Heinz, T. F. Conductivity of Solvated Electrons in Hexane Investigated with Terahertz Time-Domain Spectroscopy. *J. Chem. Phys.* **2004**, *121* (1), 394–404. https://doi.org/10.1063/1.1757442.
(19) Yan, F.; Parrott, E. P. J.; Ung, B. S.-Y.; Pickwell-MacPherson, E. Solvent Doping of PEDOT/PSS: Effect on Terahertz Optoelectronic Properties and Utilization in Terahertz Devices. *J. Phys. Chem. C* **2015**, *119* (12), 6813–6818. https://doi.org/10.1021/acs.jpcc.5b00465.
(20) Magnanelli, T. J.; Engmann, S.; Wahlstrand, J. K.; Stephenson, J. C.; Richter, L. J.; Heilweil, E. J. Polarization Dependence of Charge Conduction in Conjugated Polymer Films Investigated with Time-Resolved Terahertz Spectroscopy. *J. Phys. Chem. C* **2020**, *124* (13), 6993–7006. https://doi.org/10.1021/acs.jpcc.9b11870.
(21) Cunningham, P. D.; Hayden, L. M.; Yip, H.-L.; Jen, A. K.-Y. Charge Carrier Dynamics in Metalated Polymers Investigated by Optical-Pump Terahertz-Probe Spectroscopy. *J. Phys. Chem. B* **2009**, *113* (47), 15427–15432. https://doi.org/10.1021/jp906454g.
(22) Cunningham, P. D.; Hayden, L. M. Carrier Dynamics Resulting from Above and Below Gap Excitation of P3HT and P3HT/PCBM Investigated by Optical-Pump Terahertz-Probe Spectroscopy. *J. Phys. Chem. C* **2008**, *112* (21), 7928–7935. https://doi.org/10.1021/jp711827g.
(23) Reedijk, J. A.; Martens, H. C. F.; Brom, H. B.; Michels, M. A. J. Dopant-Induced Crossover from 1D to 3D Charge Transport in Conjugated Polymers. *Phys. Rev. Lett.* **1999**, *83* (19), 3904–3907. https://doi.org/10.1103/PhysRevLett.83.3904.

(24) Dang, M. T.; Wantz, G.; Bejbouji, H.; Urien, M.; Dautel, O. J.; Vignau, L.; Hirsch, L. Polymeric Solar Cells Based on P3HT:PCBM: Role of the Casting Solvent. *Solar Energy Materials and Solar Cells* **2011**, *95* (12), 3408–3418. https://doi.org/10.1016/j.solmat.2011.07.039.
(25) Xie, Y.; Li, Y.; Xiao, L.; Qiao, Q.; Dhakal, R.; Zhang, Z.; Gong, Q.; Galipeau, D.; Yan, X. Femtosecond Time-Resolved Fluorescence Study of P3HT/PCBM Blend Films. *J. Phys. Chem. C* **2010**, *114* (34), 14590–14600. https://doi.org/10.1021/jp912288p.
(26) Hendry, E.; Koeberg, M.; Schins, J. M.; Nienhuys, H. K.; Sundström, V.; Siebbeles, L. D. A.; Bonn, M. Interchain Effects in the Ultrafast Photophysics of a Semiconducting Polymer: THz Time-Domain Spectroscopy of Thin Films and Isolated Chains in Solution. *Phys. Rev. B* **2005**, *71* (12), 125201. https://doi.org/10.1103/PhysRevB.71.125201.
(27) Esenturk, O.; Melinger, J. S.; Heilweil, E. J. Terahertz Mobility Measurements on Poly-3-Hexylthiophene Films: Device Comparison, Molecular Weight, and Film Processing Effects. *Journal of Applied Physics* **2008**, *103* (2), 023102. https://doi.org/10.1063/1.2828028.
(28) Mahani, M. R.; Chopra, U.; Sinova, J. Engineering the Molecular Structure to Optimize the Spin Hall Signal in Organics. *arXiv:2002.11092 [cond-mat]* **2020**.
(29) Paterson, A. F.; Tsetseris, L.; Li, R.; Basu, A.; Faber, H.; Emwas, A.-H.; Panidi, J.; Fei, Z.; Niazi, M. R.; Anjum, D. H.; Heeney, M.; Anthopoulos, T. D. Addition of the Lewis Acid Zn(C6F5)2 Enables Organic Transistors with a Maximum Hole Mobility in Excess of 20 Cm2 V−1 S−1. *Advanced Materials* **2019**, *31* (27), 1900871. https://doi.org/10.1002/adma.201900871.
(30) Zhang, X.; Bronstein, H.; Kronemeijer, A. J.; Smith, J.; Kim, Y.; Kline, R. J.; Richter, L. J.; Anthopoulos, T. D.; Sirringhaus, H.; Song, K.; Heeney, M.; Zhang, W.; McCulloch, I.; DeLongchamp, D. M. Molecular Origin of High Field-Effect Mobility in an Indacenodithiophene–Benzothiadiazole Copolymer. *Nature Communications* **2013**, *4* (1), 2238. https://doi.org/10.1038/ncomms3238.
(31) Saeki, A.; Yoshikawa, S.; Tsuji, M.; Koizumi, Y.; Ide, M.; Vijayakumar, C.; Seki, S. A Versatile Approach to Organic Photovoltaics Evaluation Using White Light Pulse and Microwave Conductivity. *J. Am. Chem. Soc.* **2012**, *134* (46), 19035–19042. https://doi.org/10.1021/ja309524f.
(32) Persson, N. E.; Engmann, S.; Richter, L. J.; DeLongchamp, D. M. In Situ Observation of Alignment Templating by Seed Crystals in Highly Anisotropic Polymer Transistors. *Chem. Mater.* **2019**, *31* (11), 4133–4147. https://doi.org/10.1021/acs.chemmater.9b00888.
(33) Nienhuys, H.-K.; Sundström, V. Influence of Plasmons on Terahertz Conductivity Measurements. *Appl. Phys. Lett.* **2005**, *87* (1), 012101. https://doi.org/10.1063/1.1977213.
(34) Schmidt, M. W.; Baldridge, K. K.; Boatz, J. A.; Elbert, S. T.; Gordon, M. S.; Jensen, J. H.; Koseki, S.; Matsunaga, N.; Nguyen, K. A.; Su, S.; Windus, T. L.; Dupuis, M.; Montgomery, J. A. General Atomic and Molecular Electronic Structure System. *Journal of Computational Chemistry* **1993**, *14* (11), 1347–1363. https://doi.org/10.1002/jcc.540141112.
(35) Franco, F. C.; Padama, A. A. B. DFT and TD-DFT Study on the Structural and Optoelectronic Characteristics of Chemically Modified Donor-Acceptor Conjugated Oligomers for Organic Polymer Solar Cells. *Polymer* **2016**, *97*, 55–62. https://doi.org/10.1016/j.polymer.2016.05.025.

(36) Niskanen, M.; Hukka, T. I. Modeling of Photoactive Conjugated Donor–Acceptor Copolymers: The Effect of the Exact HF Exchange in DFT Functionals on Geometries and Gap Energies of Oligomer and Periodic Models. *Phys. Chem. Chem. Phys.* **2014**, *16* (26), 13294–13305. https://doi.org/10.1039/C4CP01165A.
(37) Zhang, L.; Zhang, Q.; Ren, H.; Yan, H.; Zhang, J.; Zhang, H.; Gu, J. Calculation of Band Gap in Long Alkyl-Substituted Heterocyclic-Thiophene-Conjugated Polymers with Electron Donor–Acceptor Fragment. *Solar Energy Materials and Solar Cells* **2008**, *92* (5), 581–587. https://doi.org/10.1016/j.solmat.2007.12.010.
(38) McCormick, T. M.; Bridges, C. R.; Carrera, E. I.; DiCarmine, P. M.; Gibson, G. L.; Hollinger, J.; Kozycz, L. M.; Seferos, D. S. Conjugated Polymers: Evaluating DFT Methods for More Accurate Orbital Energy Modeling. *Macromolecules* **2013**, *46* (10), 3879–3886. https://doi.org/10.1021/ma4005023.
(39) Farouil, L.; Alary, F.; Bedel-Pereira, E.; Heully, J.-L. Revisiting the Vibrational and Optical Properties of P3HT: A Combined Experimental and Theoretical Study. *J. Phys. Chem. A* **2018**, *122* (32), 6532–6545. https://doi.org/10.1021/acs.jpca.8b03814.
(40) Salzner, U. Electronic Structure of Conducting Organic Polymers: Insights from Time-Dependent Density Functional Theory. *WIREs Computational Molecular Science* **2014**, *4* (6), 601–622. https://doi.org/10.1002/wcms.1194.
(41) Brambilla, L.; Tommasini, M.; Botiz, I.; Rahimi, K.; Agumba, J. O.; Stingelin, N.; Zerbi, G. Regio-Regular Oligo and Poly(3-Hexyl Thiophene): Precise Structural Markers from the Vibrational Spectra of Oligomer Single Crystals. *Macromolecules* **2014**, *47* (19), 6730–6739. https://doi.org/10.1021/ma501614c.

Charge Conductivity in Donor-Acceptor Polymer Dispersions Measured with Time-Resolved Terahertz Spectroscopy

Supplementary Information:

*Timothy J. Magnanelli and Edwin J. Heilweil[1]**

Physical Measurement Laboratory, National Institute of Standards and Technology (NIST),

Gaithersburg, MD 20899, USA

Table of Contents:

1. Acronym list including studied polymer full IUPAC names
2. Parameters of bi-exponential model fits to TRTS kinetic data
3. 800 nm excitation frequency-dependent TRTS-TDS conductivity
4. Drude-Smith model fit parameters and estimated errors to TRTS-TDS frequency-dependent data
5. Bandgap and HOMO/LUMO energy level DFT predictions
6. D-A DFT HOMO/LUMO molecular orbital projections
7. D-A DFT B3LYP/6-31G infrared frequencies and intensities

1. Acronym list:

- DFT = Density Functional Theory
- THz = Terahertz
- TDS = Time domain terahertz spectroscopy
- TRTS = Time resolved terahertz spectroscopy
- FFT = Fast Fourier transform
- UV-vis-NIR = Ultraviolet-visible-near infrared electronic absorption spectrum
- CDTBTZ (C) = poly[2,6-(4,4-bis-alkyl-4H-cyclopenta[2,1-b;3,4-b']dithiophene)]-alt-4,7-(2,1,3-benzothiadiazole)
- IDTBT (I) = poly[4,9-dihydro-4,4,9,9-tetrahexadecyl-s-indaceno[1,2-b:5,6-b']-dithiophene]-alt-4,7-(2,1,3-benzothiadiazole)
- N2200 (N) = poly{[N,N′ -bis(2-octyldodecyl)-naphthalene-1,4,5,8-bis(dicarboximide)-2,6-diyl]-alt-5,5′ -(2,2′ -bithiophene)}
- PBDTTPD (PB) = poly[[5-(2-ethylhexyl)-5,6-dihydro-4,6-dioxo-4H-thieno[3,4-c]pyrrole-1,3-diyl][4,8-bis[(2-ethylhexyl)oxy]benzo[1,2-b:4,5-b′]dithiophene-2,6-diyl]]
- PCDTPT (PC) = poly[[1,2,5]thiadiazolo[3,4-c]pyridine-4,7-diyl(4,4-dihexadecyl-4Hcyclopenta[2,1-b:3,4-b']dithiophene-2,6-diyl)[1,2,5]thiadiazolo[3,4-c]pyridine-7,4-diyl(4,4-dihexadecyl-4H-cyclopenta[2,1-b:3,4-b']dithiophene-2,6-diyl)
- P3HT = poly-3-hexylthiophene
- PBTTT = poly(2, 5-bis(3-alkylthiophen-2-yl)thieno[3, 2-b]thiophene)
- GAMESS = Generalized Atomic and Molecular Electronic Structure System (version # 2019.r1.p1):

  Schmidt, M. W.; Baldridge, K. K.; Boatz, J. A.; Elbert, S. T.; Gordon, M. S.; Jensen, J. H.; Koseki, S.; Matsunaga, N.; Nguyen, K. A.; Su, S.; Windus, T. L.; Dupuis, M.; Montgomery, J. A. General Atomic and Molecular Electronic Structure System. *Journal of Computational Chemistry* **1993**, *14* (11), 1347–1363. https://doi.org/10.1002/jcc.540141112.

2. Parameters of bi-exponential model fits to TRTS kinetic data:

Table S1. Parameters for TRTS kinetic fit via an exponential and constant offset (PB), bi-exponential (I), (N), and (C), or a bi-exponential and constant offset (PC) model. Values in parenthesis correspond to 95% confidence intervals for each parameter determined via a Type A, k=1.96 nonlinear least squares error analysis.

Polymer / Pump λ (nm)	**A_1**	**τ_1 (ps)**	**A_2**	**τ_2 (ps)**
(PB) / 400	0.881 (0.832 – 0.938)	0.473 (0.223 – 0.742)	0.119 (0.100 – 0.136)	Constant (---)
(I) / 400	0.902 (0.886 – 0.919)	0.634 (0.471 – 0.811)	0.098 (0.071 – 0.128)	11.4 (7.90 – 16.9)
(N) / 800	0.931 (0.915 – 0.950)	0.583 (0.400 – 0.767)	0.069 (0.056 – 0.084)	31.4 (23.5 – 49.2)
(C) / 800	0.935 (0.890 – 0.988)	0.647 (0.056 – 1.42)	0.065 (0.019 – 0.106)	74.1 (9.7 – Constant)
(PC) / 800	0.910 (0.903 – 0.916)	0.380 (0.339 – 0.422)	0.090 (0.082 – 0.097)	12.9 (10.6 – 15.5)

Values are convolved with an error function-based instrument response function with its fit parameters omitted for brevity and limited utility. Pre-factors are normalized relative to the largest such that the sum for each polymer's trace is 1. (PB) A_2 reflects a constant offset without an associated decay time constant; attempting to fit (PB) with a bi-exponential decay (in part due to the more limited temporal range covered) leads to convergence onto a second timescale.

As described in the text, these lifetimes roughly correlate to initial charge recombination and prolonged vibrational relaxation, charge trapping, and further recombination, respectively. Given the numerous microstructural states present, these parameters are more empirical than rigorous in defining the kinetics of the co-polymer photoconduction dynamics.

3. 800 nm excitation frequency-dependent TRTS-TDS conductivity:

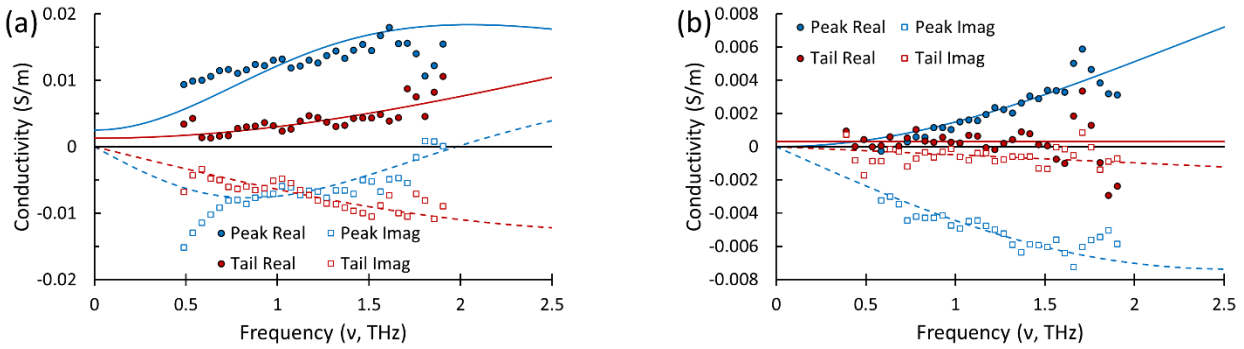

Figure S1. Complex conductivity with 800 nm photoexcitation of (a) (N) and (b) (C) D-A co-polymers to complement those shown in Figure 3 of the main text. Both datasets exhibit higher peak curvature dependence than their 400 nm counterparts, as indicated by larger τ's (scattering times) in Table S2 below. In (b) tail conductivity curvature approaches nearly flat real and near-linear negative imaginary components yielding very short scattering times.

4. Drude-Smith model fit parameters and estimated errors to TRTS-TDS frequency-dependent data:

Table S2. Drude-Smith Model best fit values to the frequency-dependent TRTS-TDS data (Fig. 3 main text) collected for each polymer at the photoconductive peak and tail (~20 ps) time delays with the specified excitation (pump) wavelength. Scattering times (τ) are in femtoseconds. Values in parenthesis constitute 95% confidence intervals for each parameter. Designation of "U" indicates that the value is an unbounded upper limit.[#]

Polymer / Pump λ (nm)	Peak C_σ	Peak τ	Peak c_1	Tail C_σ	Tail τ	Tail c_1
(C) / 400	7.62 (1.65 – U)	11.3 (1.3 – 25.0)	-0.989 (-0.997 – -0.981)	*1 *10^6* (1 - U)	0.021 (0.018 – 0.023)	-1.00 (---)
(I) / 400	3.60 (0.957 – U)	31.4 (0.1 – 79.3)	-0.865 (-0.977 – -0.817)	2.88 (0.46 – U)	13.6 (1.1 – 33.6)	-0.994 (-1 – -0.970)
(N) / 400	6.96 (1.13 – U)	11.7 (0.4 – 31.5)	-0.920 (-0.975 – -0.903)	20.9 (0.3 – U)	3.76 (0.3 – 33.1)	-0.993 (-1 – -0.986)
(PB) / 400	1.21 (0.30 – U)	24.9 (0.6 – 53.0)	-0.946 (-1 – -0.915)	3640 (2.5 – U)	0.35 (0.32 – 0.39)	-1.00 (-1 – -0.999)
(C) / 800	3.87 (2.83 – 5.42)	26.0 (22.0 – 30.4)	-1.00 (-1 – -0.991)	*1 * 10^6* (2 – U)	0.016 (0.008 – 0.021)	-1.00 (---)
(N) / 800	1.12 (0.75 – 2.01)	74.9 (50.3 – 98.4)	-0.932 (-1 – -0.838)	1.95 (0.81 – 7.24)	21.0 (10.6 – 33.3)	-0.976 (-1 – -0.961)
(PC) / 800	1.63 (1.31 – 2.13)	54.7 (46.0 – 63.4)	-0.905 (-0.942 – -0.868)	0.82 (0.18 – 24.9)	18 (2 – 40)	-0.962 (-1 – -0.932)

[#] When c_1 approaches -1, rapid scattering from boundaries or defects occurs according to the Drude-Smith model given in Equation (1) of the text. Nearly flat real conductivity with linearly negative sloping imaginary conductivity implies $\tau \rightarrow 0$ and "U" upper limits for c_1 are ill-defined because the model's three parameters are overdetermined. However, the values quoted here generated the best fit curves shown in Figure 3 of the text.

C_σ pre-factors are meant for peak to tail comparisons, not between polymers. Photoconductivity scales as $\approx C_\sigma*\tau$ except when $\tau \rightarrow 0$ and $c_1 \rightarrow -1$ at which point it shifts to scaling as $\approx C_\sigma*\tau^2$; though neither of these are steadfast; the DC-limit for real photoconductivity scales as $\approx C_\sigma*\tau*(1+c_1)$. These parameters are intended to compare the TRTS-TDS frequency-dependent conductivity between each co-polymer, though the certainty of each is limited (reasonably high uncertainty in individual parameters). τ reflects the amount of frequency-dependent curvature and peak frequency while c_1 is a measure of the extent to which the real photoconductivity approaches 0 as $\nu \rightarrow 0$ and the magnitude of the negative imaginary photoconductivity.

5. Bandgap and HOMO/LUMO energy level DFT predictions:

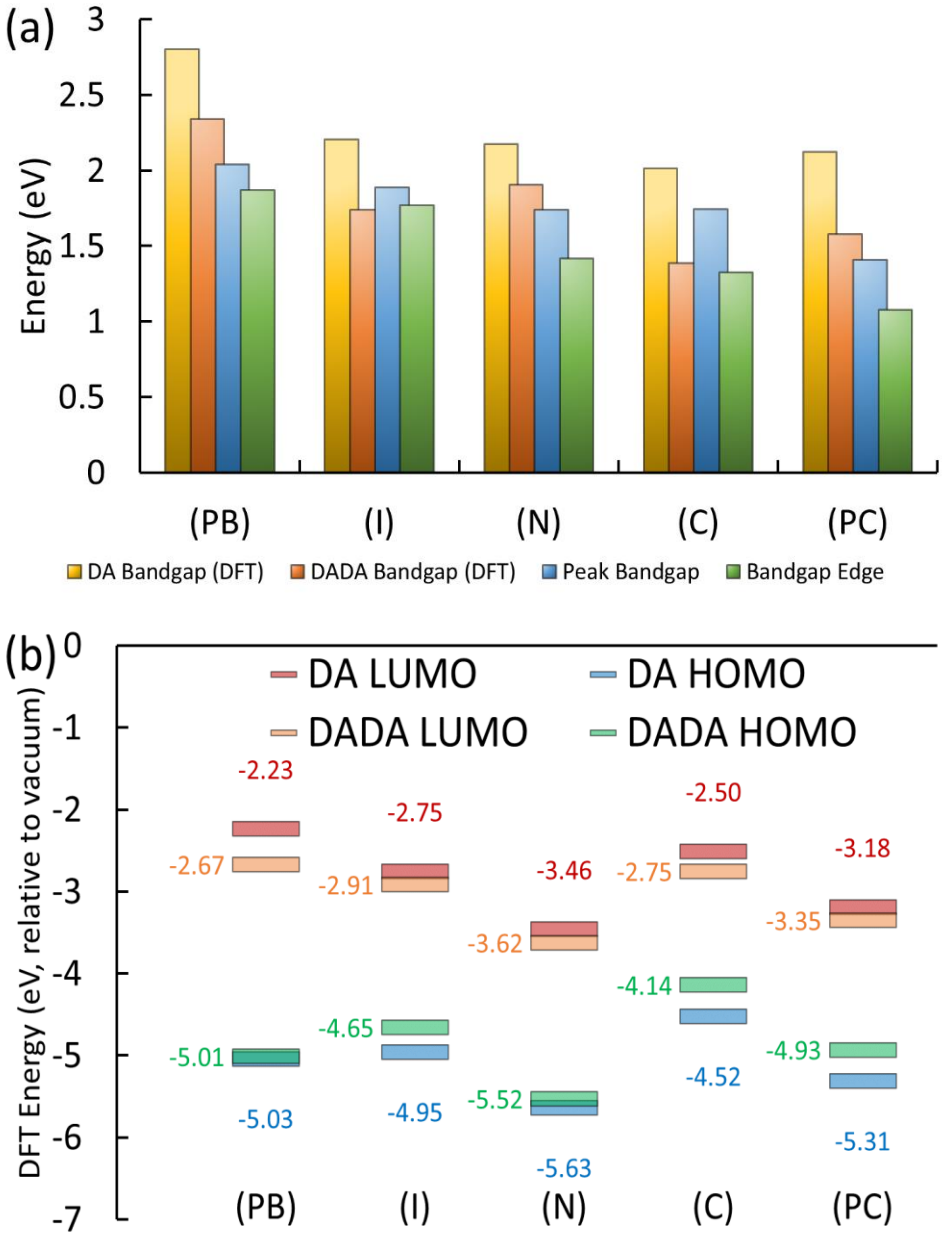

Figure S2. (a) Bandgap energies and (b) HOMO/LUMO energy levels for D-A and D-A-D-A segments for each co-polymer. DFT results were determined using GAMESS at the B3LYP/6-31G level of theory.

Figure S2(a) shows the copolymer monomeric (D-A, gold) and dimeric (D-A-D-A, orange) bandgap energies determined by DFT calculations contrasted with peak (blue) and edge (green) bandgaps measured from the UV-Vis spectra in Figure 1b. These energies provide clues as to the extent of exciton/polaron delocalization along the copolymer backbone (DFT vs. edge bandgaps) and bandwidth generated by geometric flexibility within the polymer, solvent effects, and discrete delocalization lengths based on differing local ordering (peak vs. edge bandgaps). Figure S2(b) shows the relative DFT-calculated HOMO and LUMO energy levels determined for each monomeric and dimeric unit illustrating the effects of delocalizing the excitation over an additional monomeric unit.

6. D-A DFT HOMO/LUMO molecular orbital projections:

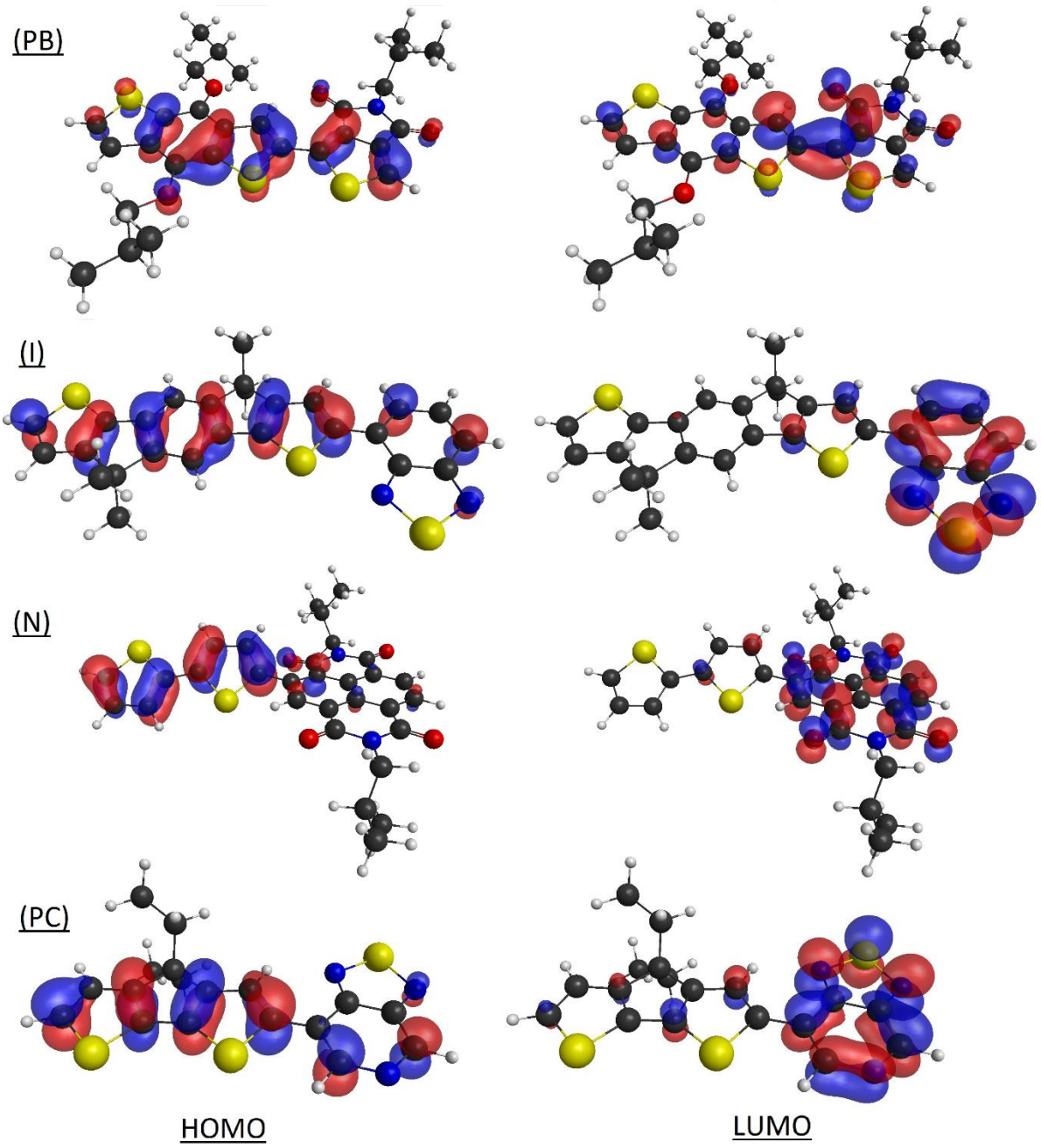

Figure S3. HOMO/LUMO orbital images for each copolymer D-A monomer

Figure S3 shows localized visualizations of the HOMO and LUMO molecular orbitals involved when photoexciting the direct bandgap transition for each copolymer. While these do not provide quite the extent of information as the D-A-D-A dimeric orbitals shown in the main text (Figure 5), they readily highlight differences between each polymer, suggesting that (PB), (N), and (I)/(PC) show coarsely different behavior based on the relative amount of localization in each donor (HOMO) and acceptor (LUMO) group. The D-A DFT energy-minimized and optimized structures shown here were used to determine vibrational frequencies (see below).

7. D-A DFT B3LYP/6-31G infrared frequencies and intensities

NOTES:

1) **Highlighted in RED in the following tables are reported back-bone D-A torsional "twist" frequencies with largest intensities (dipole change) and corresponding mode vector diagrams.**
2) **Modes 1 to 6 are rotation-translation motions; all modes yield the same A_1 output symmetry because all polymer structures are C_1 symmetry; AMU = atomic mass unit.**

CDTBTZ (C):

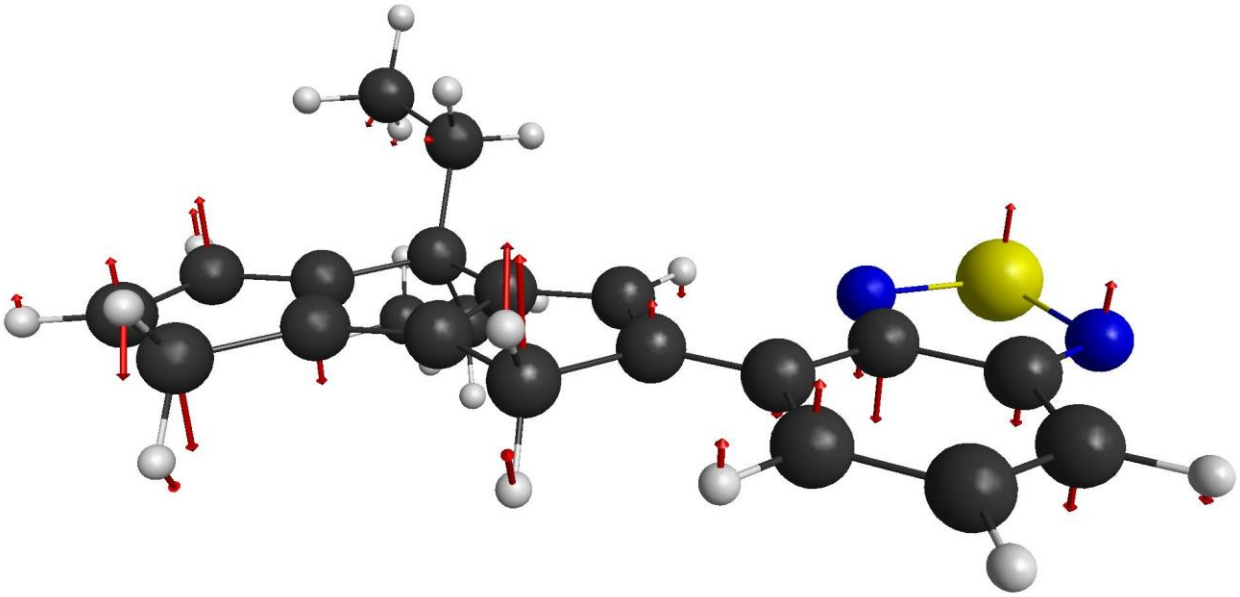

MODE	FREQUENCY (cm^{-1})	REDUCED MASS (AMU)	INTENSITY DEBYE^2/AMU-ANGSTROM^2
1	5.771	6.368028	0.005919
2	0.394	7.580501	0.000026
3	0.331	7.551228	0.000051
4	0.146	7.471995	0.000004
5	1.918	6.098295	0.002251
6	6.355	5.030372	0.004703
7	20.499	3.814724	0.003836
8	36.181	3.20466	0.00494
9	45.929	3.342916	0.000896
10	67.778	5.441432	0.005878
11	97.024	4.822726	0.00191
12	106.285	2.628259	0.011732
13	119.273	2.454449	0.007635
14	129.095	3.603555	0.0007

15	167.482	5.653523	0.013987
16	183.074	3.832846	0.001234
17	185.199	5.2072	0.00614
18	206.272	2.916123	0.010281
19	230.902	3.928985	0.007161
20	244.852	2.261411	0.005294
21	247.583	1.205134	0.000081
22	272.92	2.668223	0.013436
23	279.206	3.931596	0.174787
24	308.825	3.092875	0.00928
25	312.411	1.823313	0.061093
26	348.588	4.662172	0.02407
27	354.014	2.322467	0.272648
28	383.331	2.65746	0.160845
29	410.058	3.939309	0.01077
30	430.387	2.549337	0.082585
31	440.463	3.590596	0.007984
32	441.835	7.095428	0.506681
33	487.939	3.409812	0.196036
34	503.628	8.401157	0.267725
35	542.843	5.234744	0.809645
36	560.351	3.438672	0.011473
37	571.889	4.68816	0.182499
38	585.758	4.74647	0.175918
39	595.08	5.191287	0.040784
40	651.533	4.188902	0.006852
41	676.171	2.033996	0.58958
42	679.319	8.066838	0.13091
43	706.158	2.561118	0.077806
44	713.979	8.75171	0.086977
45	744.409	2.033173	0.25862
46	745.287	13.419616	1.171259
47	780.645	1.447861	1.058544
48	781.878	1.796855	0.080593
49	798.137	1.351661	0.016797
50	813.225	2.697091	0.098369
51	832.681	7.179071	0.08815
52	847.785	4.197829	0.412838
53	868.805	4.935003	0.556803
54	878.415	2.900596	0.123684
55	899.733	4.082901	0.152322
56	908.039	1.528687	0.04974
57	934.809	5.372065	0.232525
58	947.553	2.217122	0.110768

59	951.856	1.981845	0.414127
60	954.519	3.247372	0.208416
61	964.02	2.271263	2.217557
62	967.385	1.733193	0.036728
63	968.474	1.67844	0.025229
64	989.995	1.423949	0.138135
65	1017.591	1.360555	0.00593
66	1024.521	3.847744	0.291692
67	1059.378	2.246105	0.001831
68	1072.532	2.150187	0.306805
69	1086.119	2.25797	0.451076
70	1106.672	1.69136	0.138646
71	1108.333	2.078381	0.149045
72	1145.49	2.264347	0.096598
73	1154.284	1.732906	0.803672
74	1157.489	1.14132	0.009956
75	1173.298	2.071403	0.021612
76	1174.742	1.963489	0.448588
77	1179.103	1.257665	0.018184
78	1211.105	1.478677	0.281298
79	1219.042	2.160771	0.094019
80	1253.959	1.536098	0.397159
81	1267.031	1.668349	0.45099
82	1276.964	1.869458	0.595938
83	1304.176	2.146381	2.353231
84	1316.693	2.432723	0.458978
85	1329.912	1.196708	0.024659
86	1353.156	3.746956	2.35286
87	1366.636	1.335779	1.051324
88	1370.886	3.847944	0.054359
89	1386.054	1.266225	0.091002
90	1397.875	5.773638	5.109349
91	1406.124	1.498186	0.218511
92	1423.662	2.884829	1.064311
93	1428.517	3.198597	0.000545
94	1445.943	3.424408	4.474265
95	1457.526	1.204163	0.082248
96	1466.665	2.64188	0.068634
97	1469.691	1.262757	0.405358
98	1473.373	1.295611	0.471724
99	1484.063	1.216477	1.316191
100	1507.71	9.105499	0.303455
101	1527.51	1.171603	0.718781
102	1528.893	3.41835	6.000487

103	1536.326	4.113658	0.265587
104	1541.204	1.069127	0.105402
105	1543.783	1.097096	0.156327
106	1548.811	1.050526	0.233619
107	1558.807	1.057917	0.028996
108	1562.096	1.049041	0.235521
109	1568.424	5.443953	2.98578
110	1586.274	5.417846	0.413126
111	1599.863	5.916172	0.024626
112	1644.658	5.187581	0.65564
113	3025.796	1.061232	0.187899
114	3030.736	1.059834	0.495288
115	3034.993	1.061184	0.185318
116	3038.402	1.062155	0.142291
117	3048.536	1.037764	0.513568
118	3051.91	1.040933	1.474271
119	3067.082	1.097131	0.025417
120	3067.422	1.097563	0.543043
121	3072.416	1.099237	0.296405
122	3078.746	1.096269	0.177326
123	3111.657	1.096974	0.993315
124	3114.728	1.095948	0.657572
125	3139.397	1.100732	0.628816
126	3155.472	1.096567	1.088735
127	3185.909	1.089102	0.840146
128	3229.498	1.088012	0.247152
129	3229.65	1.089756	0.286638
130	3254.711	1.103719	0.859883
131	3258.317	1.094398	0.111802
132	3264.652	1.094954	0.017362

PCDTPT (PC):

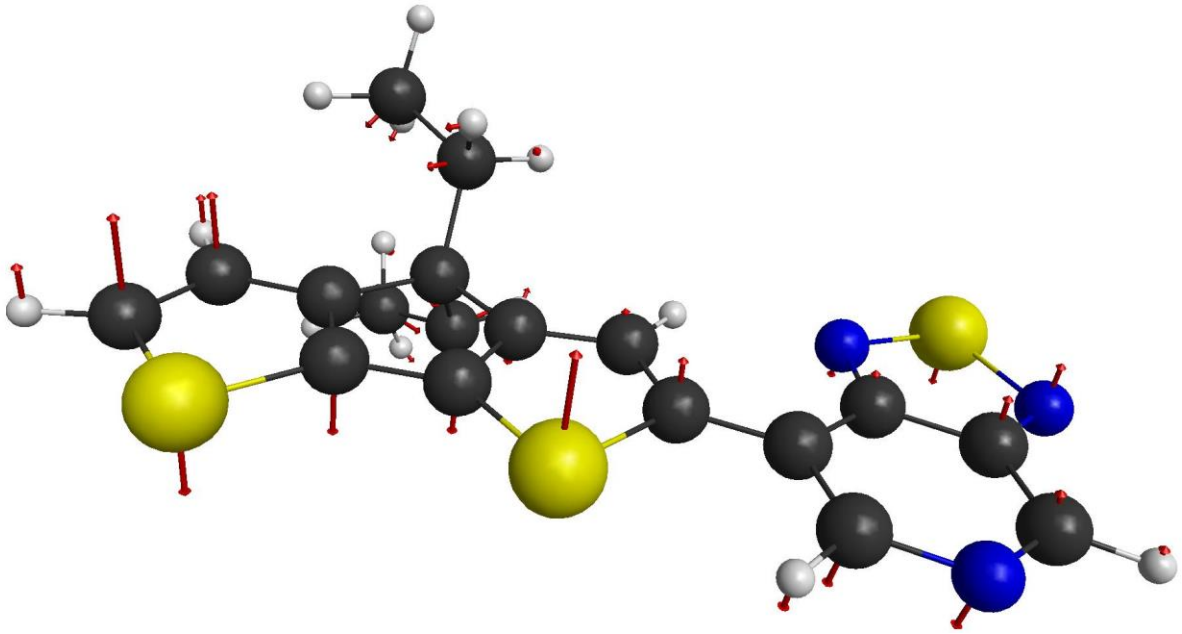

MODE	FREQUENCY (cm^{-1})	REDUCED MASS (AMU)	INTENSITY DEBYE^2/AMU-ANGSTROM^2
1	85.583	1.511113	0.003022
2	3.517	5.524974	0.008686
3	1.007	9.811902	0.00144
4	0.313	9.600051	0.000043
5	0.162	9.449556	0.000002
6	0.079	9.478245	0.000001
7	3.038	8.638329	0.003575
8	20.975	8.527917	0.000035
9	39.329	6.505199	0.001766
10	65.018	6.898922	0.003236
11	71.516	4.203528	0.002271
12	96.844	4.994649	0.000286
13	108.022	6.069296	0.003314
14	118.588	2.391023	0.001861
15	148.229	10.350463	0.011639
16	166.236	5.638117	0.016813
17	173.639	3.127438	0.001503
18	187.847	6.220737	0.001214
19	210.488	1.796963	0.003683

20	220.913	6.105452	0.020414
21	250.617	2.51179	0.000362
22	264.07	3.184097	0.005463
23	270.116	4.771159	0.016343
24	275.153	2.742653	0.012472
25	307.366	3.570143	0.008519
26	316.865	2.102852	0.01123
27	350.635	3.427325	0.032518
28	374.993	7.495624	0.036314
29	416.184	4.016115	0.010719
30	418.491	9.612934	0.145776
31	429.309	11.426618	0.398891
32	453.548	8.269495	0.245292
33	475.565	7.875369	0.04758
34	490.144	4.233809	0.039088
35	515.723	5.285938	0.036968
36	523.925	5.612665	0.230331
37	567.485	5.100781	0.254161
38	585.092	10.433976	0.208981
39	586.773	4.209392	0.129126
40	633.096	8.556046	0.07262
41	638.19	10.112123	0.091619
42	662.075	4.917876	0.037387
43	679.024	11.091738	0.518539
44	681.905	1.995778	0.987844
45	691.684	7.374388	0.292253
46	707.522	2.787061	0.132135
47	730.296	5.011836	0.518888
48	747.015	13.602037	0.724296
49	756.517	6.517039	0.04583
50	763.342	2.53011	0.50597
51	789.146	1.580681	0.052533
52	803.514	1.358855	0.023983
53	814.414	3.530566	0.059847
54	832.811	5.104185	0.032332
55	874.87	2.62864	0.881977
56	898.521	5.822309	0.077808
57	907.192	1.667844	0.72773
58	927.862	1.364789	0.211162
59	939.099	1.51	0.31595
60	945.917	7.013004	0.025152
61	951.2	1.661962	0.00222
62	963.113	1.81401	0.009257
63	976.762	2.984062	0.782129

64	1014.057	5.635439	0.050932
65	1064.178	2.482726	0.019382
66	1066.385	2.236678	0.251677
67	1109.969	1.557848	0.13967
68	1129.602	3.874902	0.246179
69	1141.347	1.672567	0.210387
70	1143.746	1.340734	0.320414
71	1152.39	5.972199	0.349249
72	1175.277	2.596152	0.023319
73	1210.775	2.079303	0.328858
74	1236.122	1.659123	0.803515
75	1262.726	1.843064	0.357653
76	1303.272	3.319834	1.057889
77	1339.981	2.35435	3.086389
78	1345.742	1.163106	0.015313
79	1357.474	6.233823	3.268556
80	1370.211	1.493242	0.507784
81	1391.123	2.574604	0.624179
82	1395.592	3.82563	1.966233
83	1397.707	1.375698	0.419517
84	1411.165	1.824855	0.306202
85	1421.402	2.230005	0.166126
86	1429.144	2.835091	0.049993
87	1448.66	1.351426	0.101724
88	1448.788	3.071813	1.215339
89	1464.739	3.106057	1.706487
90	1465.77	1.541173	0.089007
91	1475.187	6.928454	6.378605
92	1517.827	9.617327	0.617701
93	1519.027	1.084269	0.038647
94	1530.137	1.228236	0.354702
95	1530.663	3.335488	1.238847
96	1537.946	1.079158	0.009592
97	1542.947	2.675173	0.070224
98	1545.306	1.16044	0.321264
99	1556.872	2.772697	1.426803
100	1558.099	1.140658	0.189261
101	1558.841	1.221478	0.22944
102	1604.898	5.955919	2.04914
103	3029.709	1.060491	0.182276
104	3034.956	1.060149	0.547205
105	3051.077	1.037346	0.495591
106	3054.861	1.040614	1.321678
107	3076.352	1.099984	0.269593

108	3080.453	1.100017	0.268834
109	3115.273	1.096251	1.082706
110	3120.456	1.094272	0.523831
111	3141.044	1.100892	0.492298
112	3158.074	1.097915	1.031189
113	3223.93	1.089918	0.542646
114	3237.681	1.093895	0.081526
115	3248.603	1.090671	0.353228
116	3263.039	1.093011	0.05613
117	3300.952	1.098611	0.033566

IDTBT (I):

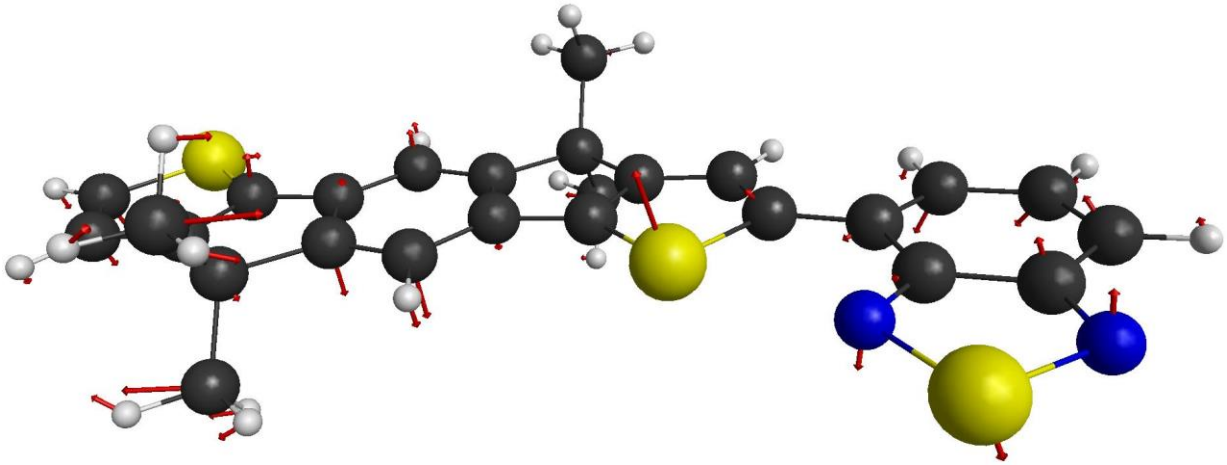

MODE	FREQUENCY	REDUCED MASS	INTENSITY
	(cm^{-1})	(AMU)	DEBYE^2/AMU-ANGSTROM^2
1	2.295	8.894621	0.001115
2	1.286	7.401464	0.000072
3	0.343	8.942843	0.000045
4	0.253	8.901616	0.000011
5	0.178	8.977329	0.000006
6	4.976	5.52898	0.00242
7	17.303	7.982697	0.006493
8	25.034	6.458944	0.003227
9	48.996	8.210703	0.007862
10	53.123	5.304998	0.011664
11	75.226	4.687352	0.015999
12	99.712	4.57232	0.00132
13	112.569	5.076301	0.001152
14	113.921	8.431899	0.003349
15	116.639	5.231658	0.001248
16	**156.835**	**4.01816**	**0.011639**
17	158.537	7.356453	0.032836
18	162.374	3.791086	0.010426
19	171.799	4.767712	0.003973
20	185.443	4.890778	0.012002
21	212.577	3.014145	0.00113
22	224.288	6.10218	0.001827
23	245.492	3.8911	0.002589
24	251.868	2.451888	0.030332
25	264.176	1.069489	0.002005

26	265.12	1.052699	0.001836
27	276.79	3.599525	0.063504
28	287.957	3.695174	0.079302
29	295.401	1.18902	0.006937
30	302.089	1.299553	0.007045
31	318.512	4.25173	0.028865
32	321.287	3.39353	0.026537
33	331.565	2.551554	0.047977
34	388.213	5.618346	0.060956
35	401.829	4.705163	0.000854
36	418.863	10.233095	0.04045
37	430.503	6.182383	0.083175
38	434.508	7.050361	0.415499
39	440.677	6.616365	0.053859
40	463.104	4.253823	0.043796
41	482.381	4.139803	0.124244
42	490.554	6.635773	0.040659
43	507.49	11.385328	0.05002
44	516.302	4.089877	0.006675
45	532.515	4.32239	0.044758
46	552.44	5.690875	0.116119
47	555.45	3.486989	0.004807
48	575.967	5.156496	0.033008
49	586.278	4.254887	0.208025
50	600.4	6.789883	0.127139
51	630.865	7.717085	0.028712
52	655.11	4.655359	0.02483
53	655.924	5.827868	0.055693
54	661.024	3.662228	0.000587
55	669.693	7.461048	0.000275
56	680.586	1.698776	1.226239
57	706.093	4.183872	0.022369
58	709.376	7.665038	0.390943
59	717.358	4.816004	0.439904
60	741.338	4.403219	0.076085
61	742.477	5.067262	0.130614
62	746.995	13.109293	0.799448
63	771.364	3.735392	0.274723
64	780.159	4.416392	0.143892
65	788.106	1.567434	0.891353
66	807.158	3.348598	0.045269
67	826.74	6.010545	0.131972
68	839.172	5.312596	0.285517
69	853.179	3.265898	0.570214

70	891.942	4.869625	0.02431
71	895.777	1.687677	0.164033
72	911.256	3.935629	0.609348
73	924.087	1.523724	0.68196
74	926.357	1.34129	0.000336
75	936.105	3.956254	0.083062
76	938.952	1.519032	0.091418
77	939.959	1.547652	0.002282
78	973.274	1.583174	0.001741
79	973.901	1.57499	0.021106
80	997.022	2.546739	0.700594
81	1004.132	2.981061	0.080535
82	1012.092	3.785414	0.056143
83	1023.526	1.355037	0.022553
84	1062.019	1.295255	0.000073
85	1062.262	1.293941	0.00033
86	1071.173	3.274565	0.385238
87	1089.745	3.410789	0.440447
88	1125.524	2.693452	0.258051
89	1129.094	2.000568	0.245077
90	1139.392	1.172867	0.040825
91	1172.836	3.417391	0.035564
92	1174.34	3.445395	0.095904
93	1183.539	2.107216	0.430814
94	1196.485	1.825318	0.017205
95	1217.99	1.463818	0.218423
96	1250.672	1.828958	1.058881
97	1259.366	2.688175	0.103309
98	1267	2.477186	0.193014
99	1271.868	3.274435	0.029005
100	1284.766	2.22711	0.08015
101	1299.439	2.409907	0.799439
102	1308.833	1.706001	0.876788
103	1366.179	4.214963	1.523819
104	1373.246	3.199965	1.108821
105	1374.547	7.591376	0.011005
106	1376.82	3.490143	0.320758
107	1389.154	3.857184	1.842344
108	1412.462	3.822125	0.179274
109	1439.666	4.594519	2.705442
110	1445.11	1.183131	0.017485
111	1445.401	1.179713	0.254361
112	1465.1	1.337777	0.224969
113	1466.536	2.012955	1.547402

114	1467.749	1.786081	0.090313
115	1471.973	4.281118	1.927566
116	1484.746	7.351972	5.601827
117	1517.129	5.669914	1.448624
118	1529.637	1.049491	0.012277
119	1529.877	1.050428	0.035047
120	1530.882	3.823597	0.340837
121	1531.946	1.059707	0.149755
122	1532.076	1.060173	0.030892
123	1539.617	3.543416	1.527584
124	1545.352	1.059414	0.271505
125	1545.624	1.092458	0.258937
126	1549.098	1.107617	0.02124
127	1550.361	1.115684	0.547322
128	1563.338	5.555193	0.051084
129	1567.971	5.640673	2.439003
130	1580.386	6.823728	0.897981
131	1601.774	9.334661	0.002986
132	1649.112	4.910158	0.271369
133	1662.056	6.779192	0.156002
134	3039.526	1.034371	0.497223
135	3040.519	1.033846	0.50112
136	3043.846	1.034707	1.180733
137	3044.962	1.034061	1.036168
138	3110.443	1.100252	0.011723
139	3111.596	1.100545	0.158011
140	3116.323	1.099527	0.922518
141	3119.354	1.100237	0.959731
142	3133.049	1.101063	0.428619
143	3135.737	1.100789	0.572579
144	3135.905	1.10078	0.500123
145	3137.777	1.100717	0.612678
146	3196.654	1.091306	0.427955
147	3203.242	1.091474	0.105012
148	3205.431	1.087311	0.739595
149	3221.644	1.090988	0.167296
150	3229.821	1.091159	0.461662
151	3238.656	1.092579	0.022788

PBDTTPD (PB):

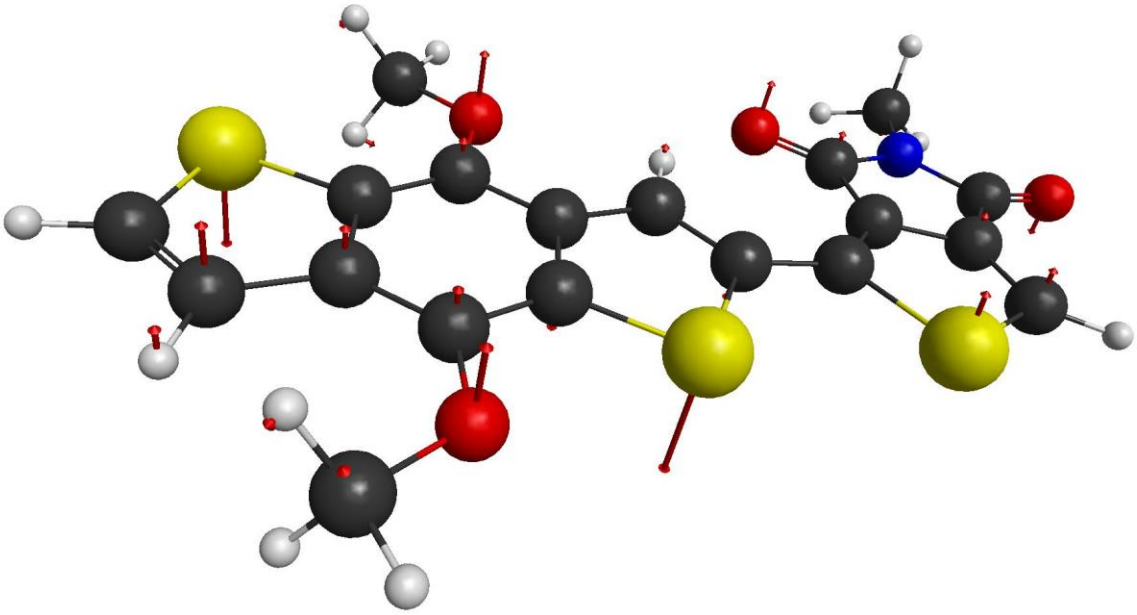

MODE	FREQUENCY	REDUCED MASS	INTENSITY
	(cm^{-1})	(AMU)	DEBYE^2/AMU-ANGSTROM^2
1	63.933	1.056826	0.013282
2	61.211	2.753044	0.169951
3	4.418	6.941456	0.000909
4	2.455	9.400215	0.002384
5	1.054	8.809362	0.004368
6	0.261	10.32975	0.000013
7	0.164	10.390238	0.000005
8	0.103	10.361084	0.000008
9	19.9	6.856103	0.00478
10	30.677	6.168975	0.00097
11	43.915	3.571122	0.102813
12	52.874	7.234799	0.008848
13	74.587	9.777781	0.070583
14	**107.887**	**13.353178**	**0.015787**
15	113.986	4.49618	0.094755
16	135.568	6.060581	0.113736
17	138.767	6.404822	0.079484
18	162.829	7.101647	0.001535
19	173.928	6.288971	0.003381
20	175.732	13.318194	0.114665
21	193.46	6.787194	0.00904
22	225.717	5.475179	0.023448

23	235.202	5.062623	0.044564
24	256.692	2.518046	0.030649
25	261.568	1.875444	0.041651
26	264.93	2.967653	0.041814
27	276.585	5.040535	0.001155
28	290.317	3.868811	0.114213
29	306.418	5.368917	0.191513
30	310.885	1.114469	0.002695
31	323.657	11.845791	0.194779
32	333.8	4.752063	0.07369
33	339.619	7.1633	0.014073
34	363.962	15.595344	0.176844
35	378.704	10.701197	0.026823
36	418.083	7.90458	0.004195
37	458.727	8.25954	0.522027
38	465.742	5.593818	0.03708
39	466.432	7.789791	0.116743
40	501.94	6.93499	0.034434
41	518.331	5.311636	0.006596
42	534.998	7.953821	0.427089
43	571.284	6.859441	0.008041
44	606.904	9.721243	0.54656
45	623.41	10.454922	0.113825
46	634.419	7.607217	0.009537
47	640.246	5.568272	0.016019
48	644.056	9.084779	0.103265
49	673.817	9.224361	0.448618
50	685.23	3.254738	0.831404
51	719.845	8.020036	0.436945
52	725.567	7.791175	0.155975
53	735.952	1.982	0.72995
54	744.987	3.154224	1.164485
55	753.928	6.731239	0.052613
56	769.846	6.277301	0.27386
57	794.5	4.939586	0.104779
58	797.219	4.965163	0.253884
59	808.112	6.165843	0.016005
60	830.894	2.164958	0.218535
61	838.142	7.602934	0.63959
62	870.965	5.822011	0.154364
63	912.437	6.293554	0.917921
64	945.629	1.355321	0.013724
65	948.945	5.459867	0.096704
66	990.478	2.640156	0.527274

67	991.785	1.883094	0.458101
68	998.762	4.187914	0.124063
69	1037.437	4.585808	4.940752
70	1086.115	5.474782	2.173928
71	1098.005	6.93019	5.381789
72	1155.39	1.213282	0.175389
73	1156.78	1.241187	0.016557
74	1173.783	1.585424	0.668494
75	1175.178	1.821008	0.980945
76	1178.381	1.338305	0.081653
77	1182.76	1.543851	0.302236
78	1206.33	1.491162	0.474986
79	1217.089	2.149619	0.059069
80	1232.923	2.25537	3.009407
81	1262.993	5.776052	1.863193
82	1286.222	2.46326	2.243973
83	1297.914	3.750008	0.44884
84	1337.663	2.58292	0.937659
85	1362.739	2.214483	2.88422
86	1365.148	4.244025	1.00589
87	1395.219	6.567265	7.063249
88	1398.803	6.565289	1.82094
89	1429.879	5.256649	8.079479
90	1464.767	4.302776	1.39234
91	1488.072	1.189236	1.472243
92	1501.231	1.329757	0.799366
93	1521.032	1.447626	1.379836
94	1531.881	1.093538	0.178987
95	1537.774	1.055435	0.313087
96	1540.302	1.054064	0.691843
97	1544.63	1.060794	0.226359
98	1549.359	3.500594	0.965749
99	1551.893	1.193189	0.385898
100	1556.279	1.055466	0.279433
101	1585.582	6.265883	1.512804
102	1600.629	10.109773	8.266143
103	1619.718	7.490257	0.377904
104	1637.072	10.250114	0.098882
105	1641.092	9.885377	0.206573
106	1701.427	11.884105	10.537568
107	1756.207	11.752499	7.546525
108	3042.21	1.03243	1.292792
109	3055.574	1.032184	0.773149
110	3065.175	1.034412	0.925822

111	3122.299	1.10534	0.820191
112	3138.35	1.100511	0.286932
113	3140.58	1.104916	0.586026
114	3172.977	1.099656	0.407269
115	3178.923	1.102004	0.075461
116	3192.874	1.10101	0.322126
117	3253.79	1.095163	0.515109
118	3271.217	1.088163	0.298153
119	3301.721	1.097023	0.215273
120	3314.819	1.099862	0.036888

N2200 (N):

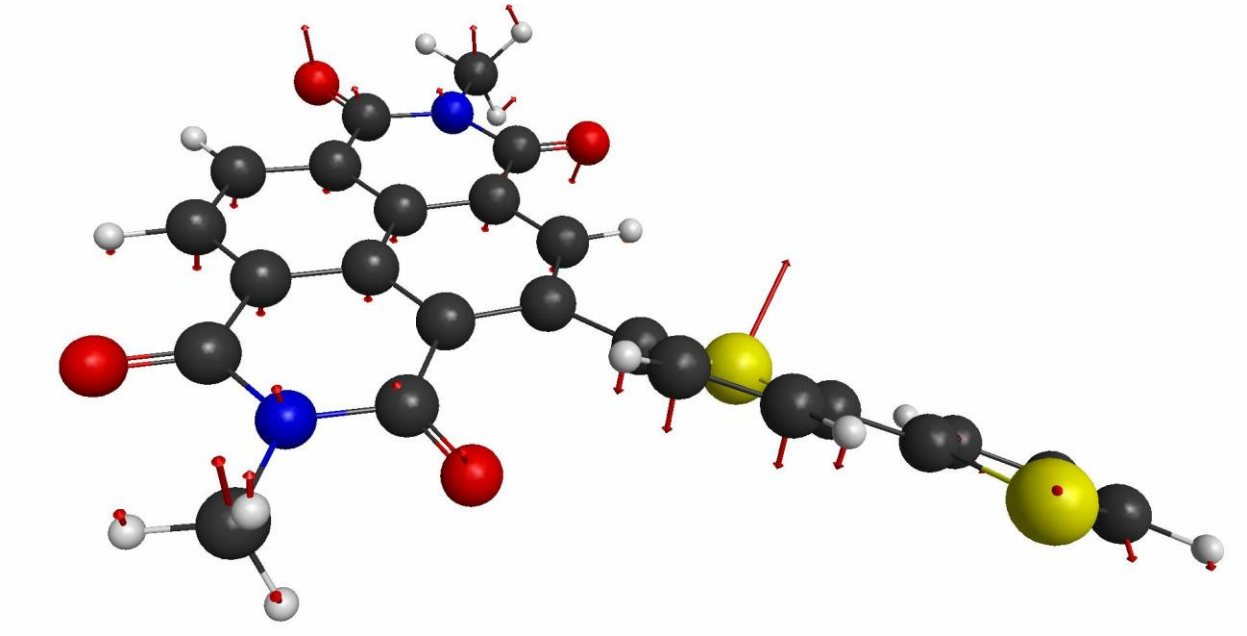

MODE	FREQUENCY	REDUCED MASS	INTENSITY
	(cm^{-1})	(AMU)	DEBYE^2/AMU-ANGSTROM^2
1	7.414	3.437241	0.001493
2	3.541	7.320936	0.000874
3	0.345	9.975318	0.000073
4	0.32	9.974335	0.000028
5	0.189	9.964539	0.000003
6	2.409	8.89715	0.001198
7	14.435	1.629305	0.014136
8	26.072	6.314557	0.004136
9	31.292	5.354614	0.001147
10	33.214	5.444612	0.014149
11	**52.723**	**9.227382**	**0.006767**
12	**55.883**	**5.934689**	**0.018424**
13	**71.283**	**5.604745**	**0.037068**
14	83.403	6.649053	0.022848
15	101.388	4.914723	0.029261
16	111.143	5.469273	0.002089
17	123.907	6.543751	0.295852
18	137.115	9.395733	0.129948
19	149.356	8.933469	0.033276
20	187.644	5.838961	0.072036
21	201.378	4.054779	0.020015

22	210.961	6.468137	0.011084
23	222.301	5.689168	0.099228
24	233.109	1.217621	0.006893
25	269.758	6.25458	0.079668
26	286.333	4.676482	0.059634
27	299.257	8.435418	0.036451
28	304.509	5.792551	0.003429
29	320.512	8.849816	0.038545
30	336.116	5.36014	0.003364
31	342.128	7.652442	0.031428
32	372.699	4.564041	0.602928
33	381.141	6.224157	0.018356
34	397.322	4.465809	0.27936
35	410.989	7.370436	1.208388
36	418.19	7.119057	0.379127
37	422.289	8.015188	0.271326
38	449.882	6.593025	0.074861
39	468.805	5.544156	0.073631
40	471.806	7.261674	0.177597
41	477.32	6.639374	0.09037
42	517.575	9.425549	0.401614
43	533.163	4.407761	0.098776
44	558.519	6.686963	0.012943
45	570.738	3.400488	0.048472
46	574.766	9.714935	0.088078
47	591.63	5.208617	0.107499
48	606.944	8.707298	0.374915
49	615.129	4.811245	0.045097
50	619.429	4.740099	0.053328
51	638.244	8.115608	0.011959
52	666.287	7.872732	0.083982
53	669.238	6.046438	0.010654
54	692.92	7.596206	0.032345
55	697.221	6.894497	0.140346
56	712.249	7.187923	0.103435
57	722.245	1.166712	1.862524
58	743.842	9.956321	0.03897
59	757.192	5.760493	0.171053
60	758.919	7.233957	0.255655
61	779.031	7.994968	0.093201
62	782.242	6.65951	0.359447
63	802.806	7.812524	0.987309
64	808.874	6.510473	0.921703
65	837.617	6.056383	0.06854

66	844.401	1.537031	1.04225
67	850.134	4.55225	0.30287
68	872.338	1.39474	0.106857
69	877.646	4.345015	0.134942
70	895.402	6.448286	0.067525
71	926.103	1.467527	0.473563
72	937.691	7.746686	0.052333
73	952.9	1.430412	0.134108
74	956.112	1.4078	0.037938
75	969.26	4.52051	0.053471
76	999.789	1.52928	0.31665
77	1015.359	4.9078	0.48389
78	1049.522	1.397032	0.008128
79	1066.855	3.173437	0.860042
80	1090.178	1.852101	0.278719
81	1095.47	2.310235	0.725398
82	1108.214	2.189	0.229595
83	1124.498	2.641805	0.108445
84	1139.371	1.166759	0.018789
85	1164.06	2.432535	0.884398
86	1174.564	1.436857	0.210171
87	1182.88	1.31908	0.113288
88	1201.69	2.354772	0.317678
89	1229.791	2.646686	5.51085
90	1241.892	3.707362	0.233043
91	1257.731	2.798911	0.435787
92	1270.081	2.127343	0.241115
93	1275.356	1.69224	0.012011
94	1284.794	3.140951	1.749577
95	1321.945	2.207202	5.579656
96	1333.837	4.203545	4.565627
97	1337.634	2.455376	2.106584
98	1340.858	3.098451	1.468298
99	1371.501	2.625405	1.060982
100	1377.495	3.29238	5.360268
101	1402.936	3.71479	1.537354
102	1409.753	3.532776	0.161462
103	1424.462	6.322902	0.209193
104	1443.515	6.468338	5.39333
105	1464.563	3.227268	2.11948
106	1489.554	1.615615	4.059286
107	1492.874	1.310485	1.467532
108	1507.292	5.14111	1.488483
109	1509.468	3.493235	1.501185

110	1516.493	5.74886	13.155238
111	1536.504	1.062852	0.304313
112	1540.246	1.07138	0.285806
113	1546.296	1.066858	0.24633
114	1551.125	1.135663	0.213477
115	1554.09	3.657225	0.36134
116	1585.511	4.622233	0.308183
117	1609.577	7.484615	1.274382
118	1626.687	7.672	5.351312
119	1633.431	6.463284	0.154516
120	1637.603	9.848239	14.589348
121	1648.19	8.003697	1.726552
122	1667.366	9.844543	1.532883
123	1680.677	9.164135	1.450845
124	1697.433	10.076991	3.087533
125	3085.54	1.036143	0.463007
126	3093.095	1.032582	0.516172
127	3159.443	1.10079	0.257217
128	3172.96	1.101921	0.256331
129	3207.419	1.103639	0.008361
130	3212.848	1.091271	0.004394
131	3230.828	1.101563	0.023484
132	3232.111	1.089148	0.406059
133	3237.012	1.090873	0.023245
134	3237.747	1.092325	0.295317
135	3247.52	1.096091	0.082415
136	3268.71	1.093119	0.014346
137	3286.584	1.09507	0.012489
138	3302.291	1.098823	0.023228

PBTTT:

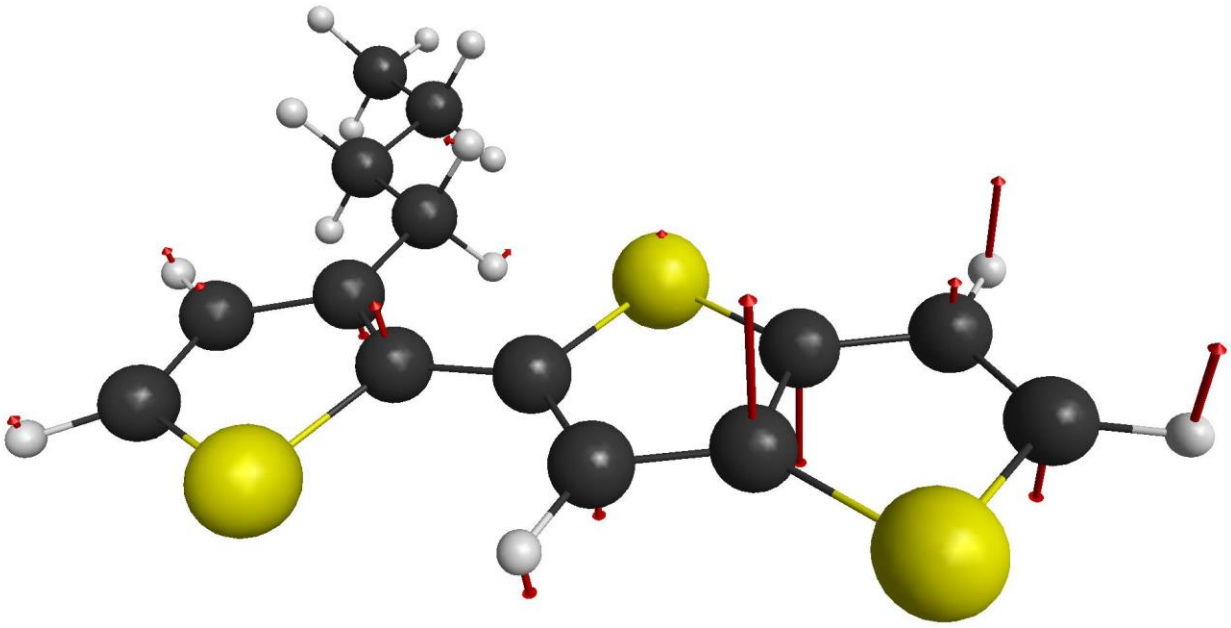

MODE	FREQUENCY	REDUCED MASS	INTENSITY
	(cm^{-1})	(AMU)	$DEBYE^2/AMU\text{-}ANGSTROM^2$
1	15.157	9.334388	0.000612
2	7.663	6.205419	0.001172
3	4.47	7.445673	0.000015
4	0.274	9.025882	0.000014
5	0.136	9.103634	0.000003
6	0.108	8.964448	0.000006
7	5.39	5.697818	0.001656
8	52.586	2.85595	0.002585
9	65.912	4.714488	0.002719
10	69.833	4.487955	0.033224
11	86.208	1.928492	0.002339
12	130.385	5.514875	0.007996
13	133.135	2.330559	0.000595
14	162.659	3.468377	0.00331
15	197.862	4.889836	0.009727
16	200.544	8.598043	0.00198
17	222.083	1.954048	0.001762
18	242.207	4.534021	0.006812
19	243.486	2.20705	0.002656
20	297.294	4.550439	0.000177
21	315.122	4.650868	0.073401

22	332.07	5.988462	0.000367
23	403.194	6.241528	0.036174
24	445.866	18.537928	0.014177
25	448.068	5.308632	0.002861
26	473.716	3.674262	0.067345
27	499.496	4.185725	0.12542
28	565.615	8.586528	0.088058
29	570.767	3.666681	0.033862
30	605.917	10.736386	0.142366
31	646.883	2.93871	0.344989
32	**649.261**	**2.84556**	**0.492231**
33	668.944	5.592134	0.087851
34	687.821	6.89615	0.052994
35	714.315	7.252121	0.431443
36	728.639	1.425846	0.449297
37	735.03	1.312494	1.650343
38	762.76	8.869642	0.469008
39	770.822	1.109756	0.229435
40	798.232	5.620233	0.154955
41	833.659	1.246618	0.006358
42	856.255	5.651986	0.282297
43	873.476	1.517384	0.409401
44	908.267	5.527993	0.844569
45	920.908	1.313601	0.038653
46	926.715	1.968539	0.065473
47	931.814	1.289857	0.008815
48	960.74	4.583149	0.150381
49	987.474	1.28366	0.05808
50	1049.449	3.467989	0.011533
51	1091.18	2.832069	0.001036
52	1130.395	1.201285	0.056561
53	1142.213	2.029011	0.160766
54	1149.206	1.242368	0.114267
55	1169.32	1.467571	0.000712
56	1189.902	2.2431	0.006248
57	1230.199	3.45355	0.025374
58	1249.692	1.509057	0.439054
59	1277.806	2.416385	0.061763
60	1284.177	1.353509	0.00045
61	1329.578	1.462061	0.062237
62	1353.462	1.176027	0.010343
63	1368.044	2.534863	0.029496
64	1370.292	1.068707	0.004497
65	1388.105	2.759393	0.009043

66	1401.418	1.93961	0.121342
67	1419.893	1.750917	0.02697
68	1428.693	1.442609	0.02958
69	1460.26	1.209574	0.050225
70	1494.521	8.205736	0.408816
71	1510.034	5.912426	0.363098
72	1527.642	1.13095	0.132603
73	1536.213	1.057453	0.081398
74	1542.236	1.062978	0.08703
75	1545.278	1.112894	0.126529
76	1545.667	4.522016	0.295979
77	1557.803	1.098485	0.103254
78	1566.543	5.364213	0.286803
79	1614.033	7.033628	0.239823
80	2982.268	1.071371	0.293083
81	3017.253	1.063903	0.159381
82	3032.3	1.061501	1.083523
83	3038.972	1.035895	0.925783
84	3064.469	1.091424	0.073157
85	3075.339	1.088208	0.260768
86	3093.44	1.099427	0.766308
87	3107.784	1.09883	1.147765
88	3124.574	1.10124	1.587302
89	3240.758	1.091717	0.192669
90	3242.839	1.093094	0.219161
91	3246.092	1.088922	0.28599
92	3287.397	1.100076	0.005962